NUSC Technical Report 7923
14 May 1987

Global Model for Sound Absorption in Sea Water

R. H. Mellen
PSI - Marine Sciences

P. M. Scheifele
Combat Systems Analysis Staff

D. G. Browning
Surface Ship Sonar Department

Naval Underwater Systems Center
Newport, Rhode Island / New London, Connecticut

Preface

This report was prepared for the Naval Underwater Systems Center, Principal Investigator LT P. M. Scheifele (Code 61M). The report was prepared in large part by Dr. R. H. Mellen, Planning Systems Incorporated - Marine Sciences and co-authored by LT P. M. Scheifele, and D. G. Browning of the Naval Underwater Systems Center, New London Laboratory.

The authors wish to acknowledge T. Bell, B. Fisch, G. Smith, Dr. D. Klingbeil, J. Hanrahan, C. DeVoe, J. Doebler, and J. Dlubac for their guidance and assistance with the direction and format of the reports.

Reviewed and Approved: 14 May 1987

L. Freeman
Head, Surface Ship Sonar Department

Head, Combat Systems Analysis Staff

UNCLASSIFIED
SECURITY CLASSIFICATION OF THIS PAGE

AD A181-658

REPORT DOCUMENTATION PAGE

1a. REPORT SECURITY CLASSIFICATION UNCLASSIFIED	1b. RESTRICTIVE MARKINGS
2a. SECURITY CLASSIFICATION AUTHORITY	3. DISTRIBUTION / AVAILABILITY OF REPORT Approved for public release; distribution is unlimited.
2b. DECLASSIFICATION / DOWNGRADING SCHEDULE	
4. PERFORMING ORGANIZATION REPORT NUMBER(S) TR 7923	5. MONITORING ORGANIZATION REPORT NUMBER(S)
6a. NAME OF PERFORMING ORGANIZATION Naval Underwater Systems Center 6b. OFFICE SYMBOL (If applicable) Code 61M	7a. NAME OF MONITORING ORGANIZATION
6c. ADDRESS (City, State, and ZIP Code). New London Laboratory New London, CT 06320	7b. ADDRESS (City, State, and ZIP Code)
8a. NAME OF FUNDING / SPONSORING ORGANIZATION 8b. OFFICE SYMBOL (If applicable)	9. PROCUREMENT INSTRUMENT IDENTIFICATION NUMBER
8c. ADDRESS (City, State, and ZIP Code)	10. SOURCE OF FUNDING NUMBERS PROGRAM ELEMENT NO. / PROJECT NO. / TASK NO. / WORK UNIT ACCESSION NO.

11. TITLE (Include Security Classification)
GLOBAL MODEL FOR SOUND ABSORPTION IN SEA WATER

12. PERSONAL AUTHOR(S)
R. H. Mellen (PSI), P. M. Scheifele and D. G. Browining (NUSC)

13a. TYPE OF REPORT	13b. TIME COVERED FROM ____ TO ____	14. DATE OF REPORT (Year, Month, Day)	15. PAGE COUNT
		1987 May 14	

16. SUPPLEMENTARY NOTATION

17 COSATI CODES			18. SUBJECT TERMS (Continue on reverse if necessary and identify by block number)
FIELD	GROUP	SUB-GROUP	

19 ABSTRACT (Continue on reverse if necessary and identify by block number)

The attenuation term in the sonar equation for propagation loss can be taken to include all losses that are proportional to range. Absorption in the medium is usually the dominant mechanism; however, interface scattering, volume scattering and diffraction can also become important components under certain conditions.

Sound absorption in sea water is an order of magnitude greater than in fresh water at sonar frequencies. Resonator experiments in the 1950's identified the mechanism as an ionic relaxation of magnesium sulfate in the 100 kHz range. Sea experiments in the 1960's showed another anomaly in the 1 kHz range. T-jump measurements in the 1970's showed that boric

20. DISTRIBUTION / AVAILABILITY OF ABSTRACT ☐ UNCLASSIFIED/UNLIMITED ☒ SAME AS RPT ☐ OTIC USERS	21. ABSTRACT SECURITY CLASSIFICATION UNCLASSIFIED
22a NAME OF RESPONSIBLE INDIVIDUAL P. M. Scheifele	22b. TELEPHONE (Include Area Code) (203) 440-6589 22c. OFFICE SYMBOL Code 61M

DD FORM 1473, 84 MAR

83 APR edition may be used until exhausted
All other editions are obsolete.

SECURITY CLASSIFICATION OF THIS PAGE
UNCLASSIFIED

19. ABSTRACT (Cont'd.)

acid is involved. Details of the mechanism were investigated using the resonator method in the 1980's. Other relaxations were also discovered but the only one of these that plays a significant role in sea water is the magnesium-carbonate relaxation.

A three-relaxation model of sea water absorption has been developed based on both laboratory and sea experiments. The main feature of the new model is the pH dependence of two components: boric acid and magnesium carbonate. In the nominal sea-water pH range 7.7-8.3, the low-frequency absorption changes by nearly a factor of 4. Model tests, using available sea data and archival pH values, show good agreement.

Error analysis indicates that predictions can be expected to be accurate to within ±15%, providing that local pH is known to within ±0.05 units. Variability of pH with depth is usually much larger than this. Integration of loss over ray paths for typical depth profiles indicates that adequate accuracy can be attained by using axial values for sound channels and 2 km depth values for convergence zones. A global model with contour charts for estimating these values throughout the World Ocean is presented.

Table of contents page

Introduction

Acoustic propagation loss is a critical factor in the design, performance and effectiveness of all submarine and surface-ship sonar systems. The attenuation term in the sonar equation for propagation loss is taken here to include all the mechanisms for which the loss is proportional to range. Absorption in the medium is generally the dominant mechanism.

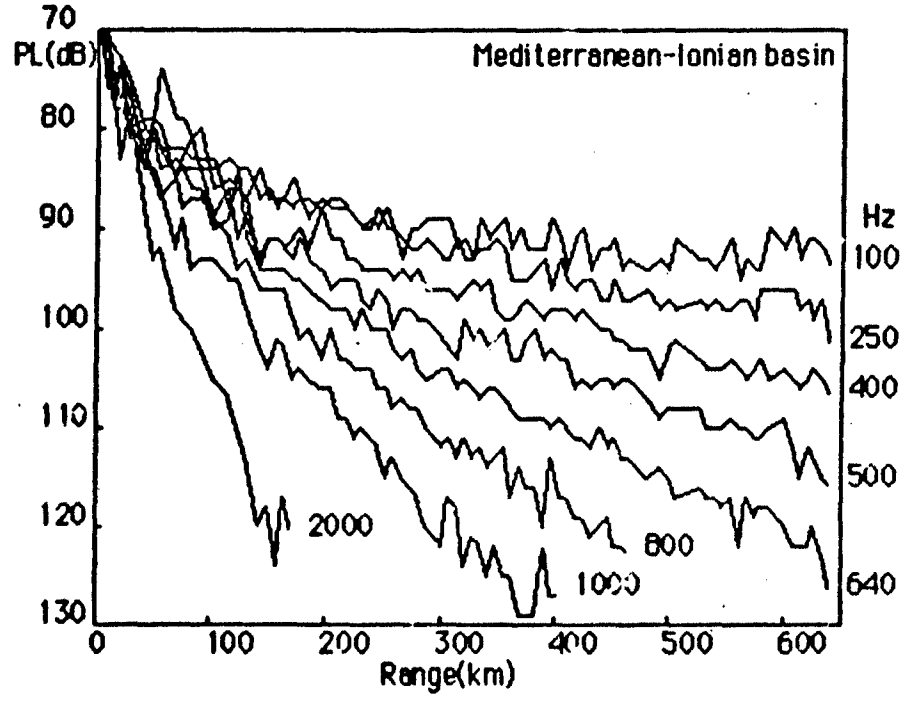

Figure 1: Mediterranean propagation loss data.

Absorption tends to increase as the square of the frequency and this limits the maximum useable frequency for any given range. The situation is illustrated by the results of a recent sound-channel experiment in the Mediterranean Sea [1]. The curves of propagation loss in dB// 1m shown in Figure 1 clearly demonstrate the increasing effects of absorption with increasing signal frequency.

In order to deal quantitatively with limitations imposed by attenuation, the other loss mechanisms can not be neglected. Internal scattering and diffraction loss are important in some of the experiments to be discussed. However, they are incidental to the main purpose of the report, which is to develop a predictive global model for sound absorption in sea water that includes the dependence on environmental factors.

Background

The 1935 Naval Research Laboratory report by Stephenson [2] appears to be the first to recognize that sound absorption in sea water is very much greater than in fresh water. However, it was not until after WWII, after the anomaly had been clearly established by extensive field measurements, that efforts were undertaken to determine the cause.

Laboratory studies in the MHz range had shown that pure water followed the classical law of absorption proportional to frequency-squared, but the magnitude was four times greater than that predicted by shear viscosity alone. This anomaly was eventually attributed to the additional effects of bulk viscosity. When extrapolated to the 10-100 kHz range, the predicted coefficients were still lower than the sea data by an order of magnitude.

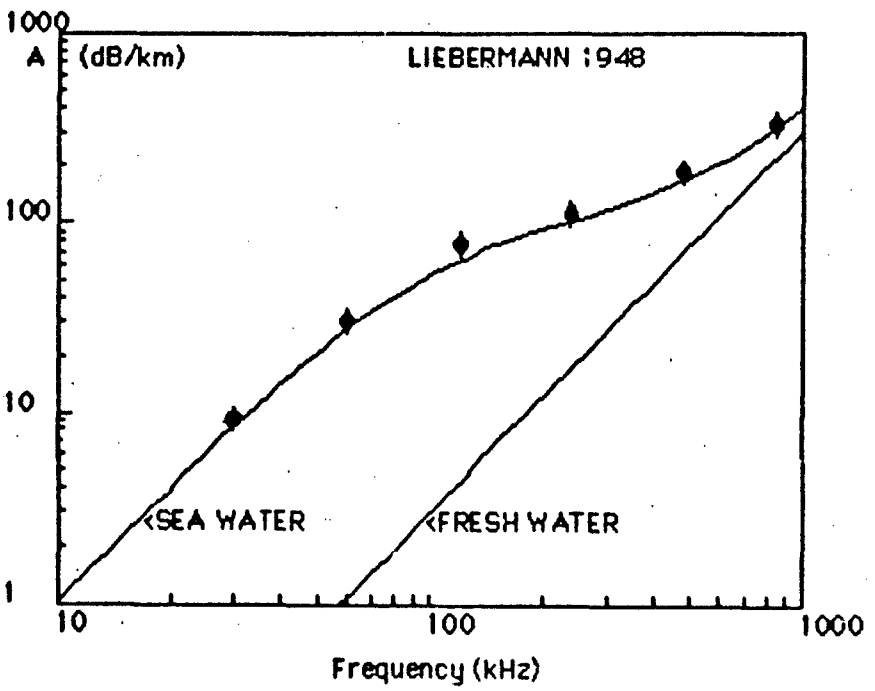

Figure 2: Liebermann's experiment.

In 1948, Liebermann [3] reported experiments comparing fresh and sea-water absorption in the band 10 kHz to 1 MHz. Data obtained in a fresh-water reservoir agreed with high-frequency laboratory measurements. Below 100 kHz the sea data were also in agreement with reported ocean results; however, they fell off at higher frequencies, approaching the fresh-water values near 1 MHz as shown in Figure 2. Liebermann proposed ionic relaxation of NaCl as a candidate mechanism.

Relaxational absorption can occur in aqueous solutions as the result of pressure-dependent chemical equilibria. Density of the medium changes according to LeChatelier's principle; i.e. if one species is smaller than the other, increasing pressure will drive the reaction in the direction of the smaller species and the compressibility is thereby altered. The rate of the process is governed by the time constant of the reaction. Therefore, the sound speed c becomes complex and acoustic waves decay with range.

Better insight is gained from the complex wavenumber $k=2\pi f/c$. Since dispersion is very small (<<1 m/s), it can be neglected and the wavenumber can be approximated as $k \approx 2\pi f/c_0 + iA$ where c_0 is constant. Then we have $A=a_r f_r f^2/(f^2 + f_r^2)$ where A is the loss per unit distance and f_r and a_r are the relaxation-frequency and amplitude parameters.

It can shown that $A_{max} = a_r f_r = k' [Z] \Delta V^2 \rho c / 2R(T+273)$ where k' is the forward rate constant, [Z] is the concentration of the species Z, ΔV is the volume change of the equilibrium involved, R is the "gas constant" and T is the temperature in °C. The equilibrium constant for the reaction is given by $K=k'/k'$ where k' is the reverse rate constant.

Various types of equilibria may be involved and each one has a specific formula for relaxation frequency and volume change. The examples listed below are typical and can easily be extended to other cases.

The simplest type is the single-step equilibrium:

$$Z \leftrightarrow Z' \qquad f_r = (k' + k')/2\pi \qquad K = [Z]/[Z'].$$

In ionic solutions like sea water, equilibria can be of the type:

$$Z \leftrightarrow X^+ + Y^- \qquad f_r = (k' + k'([X^+] + [Y^-]))/2\pi \qquad K=[Z]/[X^+][Y^-]$$

Generally, the single-step equilibria are diffusion-controlled and too fast to cause sound absorption in the sonar frequency range. Slower ionic relaxations in sea water can usually be modeled as two-step equilibria, which have two distinct relaxation frequencies. The second step is rapid and the associated high-frequency relaxation does not contribute to the absorption at sonar frequencies and the slow first step controls the relaxation frequency in question. This type can be represented as:

$$Z \leftrightarrow Z' \leftrightarrow X^+ + Y^-$$

Then $f_r = (k'_1 + k'_1 q/(1+q))/2\pi$ and $\Delta V = \Delta V_1 + \Delta V_2/(1+q)$

where $q = K_2([X^+] + [Y^-])$, $K_1 = [Z]/[Z']$ and $K_2 = [Z']/[X^+][Y^-]$

Another type that will be encountered is the exchange equilibrium:

$$XY^- \leftrightarrow YX^- \qquad f_r = (k'([X]+[Y^-]) + k'([Y]+[X^-]))/2\pi \qquad K=[X][Y^-]/[X^-][Y]$$

The formula for A_{max} remains the same for all equilibria except that the concentration factor [Z] becomes $[X][Y^-]$ for the exchange type.

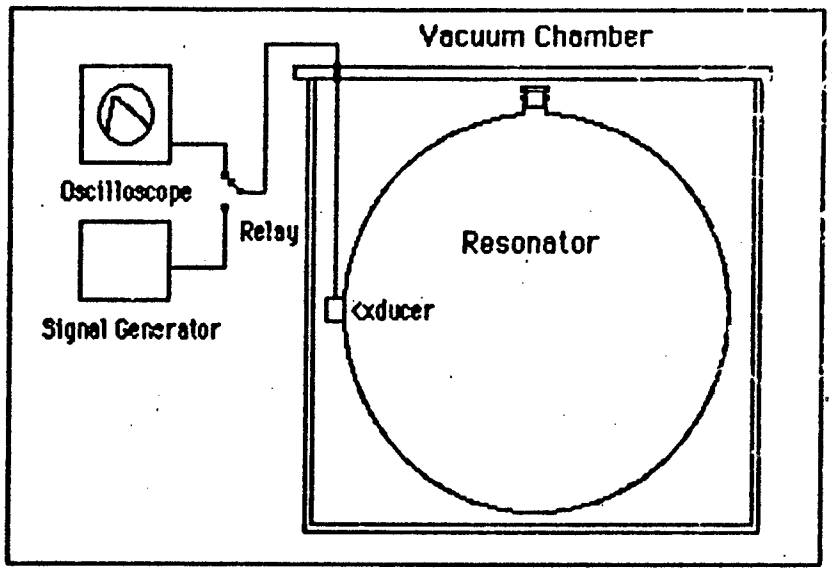

Figure 3: Resonator apparatus.

In 1949, Leonard et. al. [4] reported initial results of a laboratory study to determine what equilibrium is involved in sea-water absorption. Their apparatus consisted of a spherical resonator as illustrated in Figure 3. The resonator was suspended in a vacuum chamber by wires to minimize any residual losses caused by acoustic radiation. The useable frequency range was 25-500 kHz and values of $Q > 10^5$ were realized in pure water at lower frequencies.

In the resonator method, the transducer can serve as both transmitter and receiver. The sphere is excited specific resonant frequencies. Radial resonances usually give the lowest residual losses and they can usually by located by calculation. However, because the resonator is not perfectly spherical, the resonances are hardly ever simple. The resonant frequencies shift with changes in sound speed caused by variation of temperature or the addition of chemicals. Interference effects among adjacent modes can result in rapid changes in residual loss and this limits the accuracy of the measurements.

Losses are determined by switching the transducer from the transmit to the receive mode and measuring the rate of decay in dB/s. The system is first calibrated using distilled water. The excess losses of the various chemical constituents are then determined by subtracting the calibration values from the measured values. The losses in dB/km are calculated by dividing by the sound speed.

The experiments of Leonard et. al. showed no effects for NaCl alone. The salt responsible for the excess absorption in sea water was determined to be magnesium sulfate ($MgSO_4$).

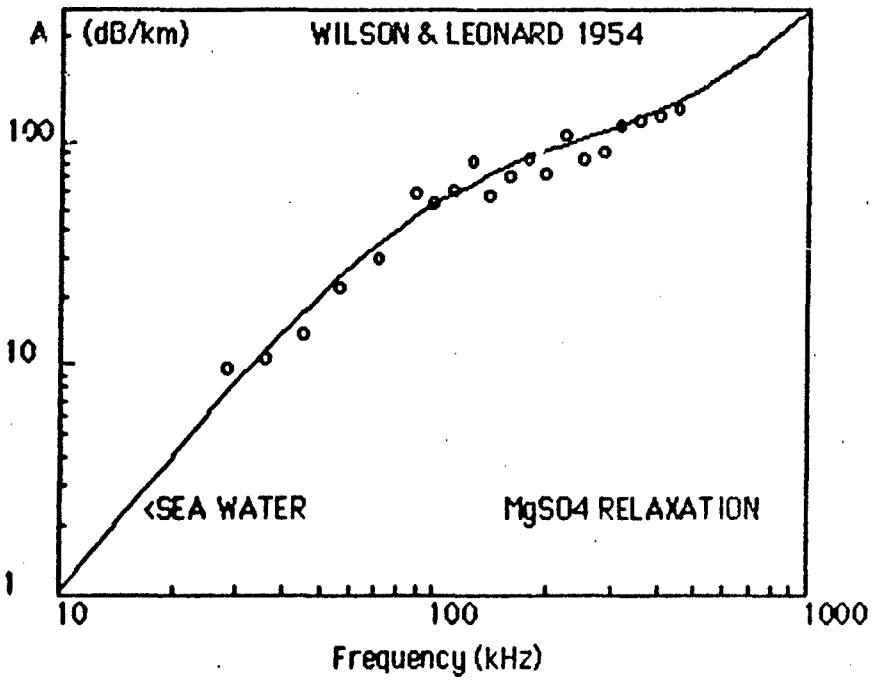

Figure 4: Resonator measurements of Wilson and Leonard.

Results of a more detailed study of magnesium sulfate by Wilson and Leonard [5] appeared in 1954 and are illustrated in Figure 4. The earlier conclusions were confirmed and dependence on concentration was also investigated. It was found that interactive effects of NaCl actually causes a reduction in sea water absorption.

In 1953, Kurtze and Tamm [6] also reported results of similar resonator experiments confirming Leonard's findings. Several possible mechanisms were proposed; however, it was not until 1962 that a definitive analysis by Eigen and Tamm [7] disclosed the details of the multistep equilibrium involved. Two or more steps were indicated by the fact that the relaxation frequency increases with concentration up to a limiting value.

The essential acoustic properties of the relaxation can be modeled in a more simplified form as the two-step equilibrium:

$$(MgSO_4)_I \leftrightarrow (MgSO_4)_{II} \leftrightarrow Mg^{2+} + SO_4^{2-}$$

The slower first step involves only a structural change and this controls the relaxation frequency of the absorption process in question. The second relaxation is very rapid and its contribution is negligible. The reduction effect of NaCl can be attributed to the coupling effects of another rapid equilibrium involving the ion-pair $NaSO_4^-$.

In 1962, Schulkin and Marsh [8] introduced the first practical formula for sound absorption in sea water. The approximation was based on the laboratory resonator experiments and extensive sea measurements in the frequency range 2-25 kHz.

The parameters involved in the S&M formula are temperature, salinity and pressure. The pressure factor of magnesium sulfate was assumed to be the same as the pure water value obtained by laboratory measurements at high pressures and is given by $(1-6.54\times10^{-4}P)$ where P is the ambient pressure in atmospheres. An alternative approximation is $10^{-D/35}$ where D is the depth in km. The S&M formula can then be written:

$$A=\{0.02\,S\,f_r\,f^2/(f_r^2+f^2)+0.03\,f^2/f_r\}\times10^{-D/35}\ \text{dB/km}$$

$$f_r=59\times10^{T/49}\ \text{kHz}$$

where f_r is the relaxation frequency of magnesium sulfate, S is salinity in parts per thousand (ppt) and T is temperature in °C. The first term is the magnesium sulfate component and the second is the pure water component. The temperature dependence of pure water has been approximated by using the relaxation frequency as a parameter, which makes both coefficients equal.

For the parameter values S=35, T=4°C and D=0, the formula becomes:

$$A\approx 50\,f^2/((71)^2+f^2)+0.0043\,f^2\ \text{dB/km}$$

which reduces to $A\approx0.01\,f^2$ dB/km for $f\ll f_r\approx71$ kHz.

The S&M formula was adequate for the sonar problems of that period; however, attention in underwater acoustics subsequently shifted to longer ranges and lower frequencies and the accuracy of extrapolating beyond the data base was questioned. A number of sea experiments were then carried out which indicated anomalous behavior at much lower frequencies.

Low-Frequency Anomaly

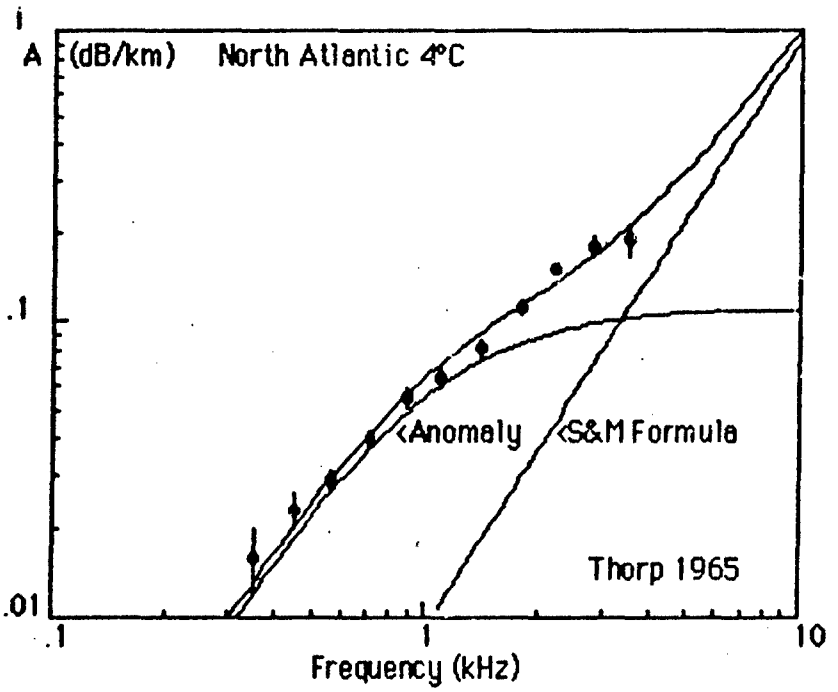

Figure 5: Thorp's data and 2-component model.

In 1965, Thorp [9] carried out a sound-channel propagation experiment in the Bermuda-Eleuthera area over a 500 km track. Measurements were made at 1200 m near the sound-channel axis using explosive sources. Results showed a clear anomaly below 3 kHz as seen in Figure 5. Comparison with other earlier data confirmed his conclusion that the values were an order of magnitude greater than that predicted by the Schulkin-Marsh formula. In a later paper, Thorp and Browning [10] modeled the anomaly, adding a 1 kHz relaxation component to the absorption formula. The formula used in the data-fit of Figure 5 is given by:

$$A = 0.009\, f^2 + 0.11\, f_r\, f^2/(f_r^2 + f^2)\ \text{dB/km} \quad (f_r = 1\ \text{kHz}).$$

The first term is the magnesium sulfate component approximated for frequencies well below the relaxation frequency 71 kHz. The second term is the anomalous component. The pure water component is negligible in this frequency range and has been omitted.

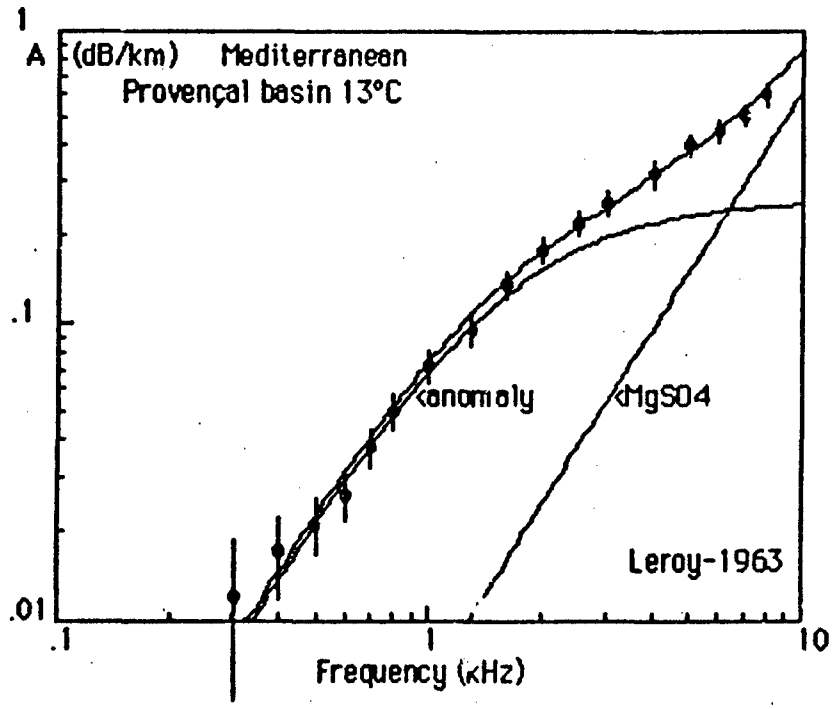

Figure 6: Leroy's data and 2-component model.

Another propagation experiment was carried out in the Provençal Basin of the Mediterranean Sea by Leroy [11]. In this case, propagation loss was measured over a single refraction path and not in the sound channel. The range was therefore limited to 40 km.

Leroy's results also showed a similar anomaly of roughly the same magnitude as Thorp but with a significantly higher relaxation frequency.

The formula used by Leroy for the data-fit is given by:

$$A = 0.006\, f^2 + 0.155\, f_r\, f^2/(f_r^2 + f^2)\ \text{dB/km} \qquad (f_r = 1.7\ \text{kHz})$$

The first term is the magnesium sulfate component and the coefficient is in reasonable agreement with the S&M formula for the 13°C temperature. The coefficient of the anomaly is also significantly greater than Thorp's value.

Under the assumption that the anomaly is truly a relaxation process, the difference between the two relaxation frequencies can be attributed to the difference in temperatures. However, the difference in coefficients is somewhat greater than the estimated experimental error. Despite this disagreement, a second relaxation still seemed to be the most promising explanation of the anomaly.

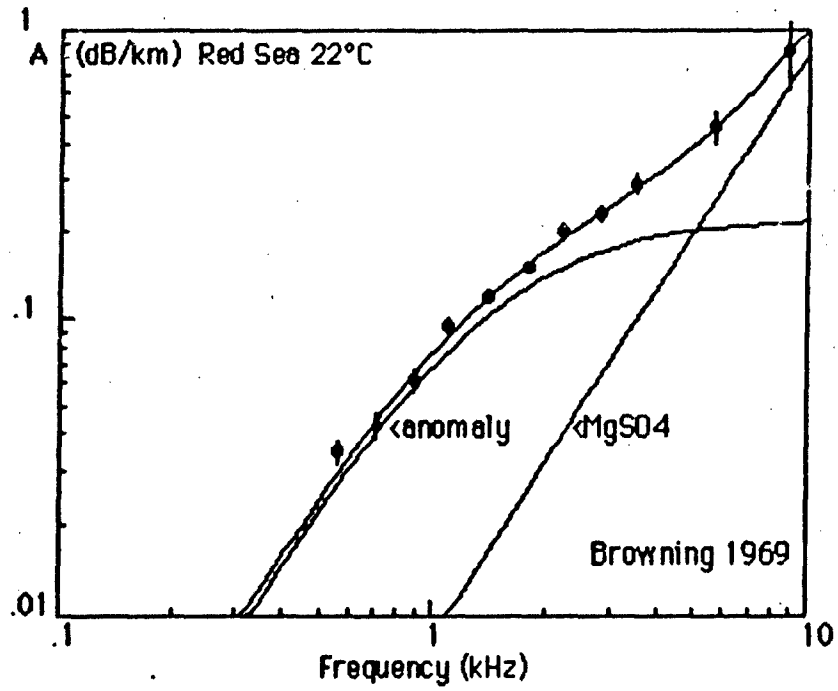

Figure 7: Red Sea data and 2-component model.

Browning et. al. carried out a number of sound-channel experiments to test the relaxation hypothesis. In the Red Sea experiment of 1969 [12], the track was 300 km long and the water depth was 750 m or greater. Sound-velocity profiles showed a strong sound channel with axis near 200 m. The ambient temperature was 22°C on the axis and 30°C at the surface. Measurements were made axis-to-axis using SUS charges at 200 m depth.

Relaxation frequency can be expected to increase exponentially with temperature over the limited range of temperatures encountered in the sea. Based on extrapolation of the Thorp and Leroy values, the expected relaxation frequency in the Red Sea experiment was approximately 2 kHz. However, the curve fit of Figure 7, indicated a significantly lower value.

The Red Sea formula used in the data-fit is given by:

$A = 0.008\, f^2 + 0.148\, f_r\, f^2/(f_r^2 + f^2)$ dB/km $\quad (f_r = 1.5$ kHz)

The anomaly coefficient is clearly in better agreement with Leroy's value than that of Thorp and the magnesium sulfate coefficient is significantly greater that predicted by the S&M formula.

The relaxation hypothesis remained promising despite inconsistencies; however, it was not until 1973 that it was firmly established by an entirely different experimental technique; i.e. the T-jump method.

T-Jump Measurements

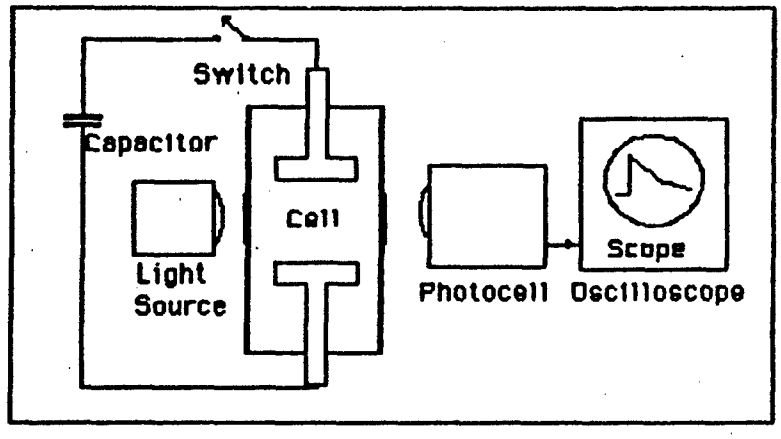

Figure 8: Temperature-jump apparatus.

In 1973 Yeager et. al. [13] reported results of T-jump experiments with both synthetic and actual sea-water. In this method, a very rapid rise in temperature is produced by discharge of the capacitor through electrodes in the cell containing the solution, as shown in Figure 8. A chemical pH indicator was used. Light transmission to the photocell measures the pH change produced by the temperature jump and the relaxation frequency is determined from the rate of change as measured by the oscilloscope.

Sea water showed the 1 kHz relaxation, proving that the equilibrium is the acid/base type. Synthetic sea water (SSW) was tested by addition of chemicals to distilled water according to the formula:

Constituent	Concentration (mM)
Sodium Chloride (NaCl)	400
Magnesium Sulfate ($MgSO_4$)	35
Magnesium Chloride ($MgCl_2$)	20
Calcium Chloride ($CaCl_2$)	10
Sodium Bicarbonate ($NaHCO_3$)	2.5
Boric Acid ($B(OH)_3$)	0.5

where concentrations are in millimoles per liter (mM). The constituent responsible was identified as boric acid. The relaxation rate was found to increase with concentration and temperature but pH had negligible effect.

In aqueous boric acid, the ionization mechanism is believed to be:

$$B(OH)_3 + OH^- \leftrightarrow B(OH)_4^-$$

where OH^- is the hydroxyl ion and $B(OH)_4^-$ is the borate ion. However, the concentration of the carbonate ion is much greater in sea water and an exchange reaction was proposed as the more likely mechanism.

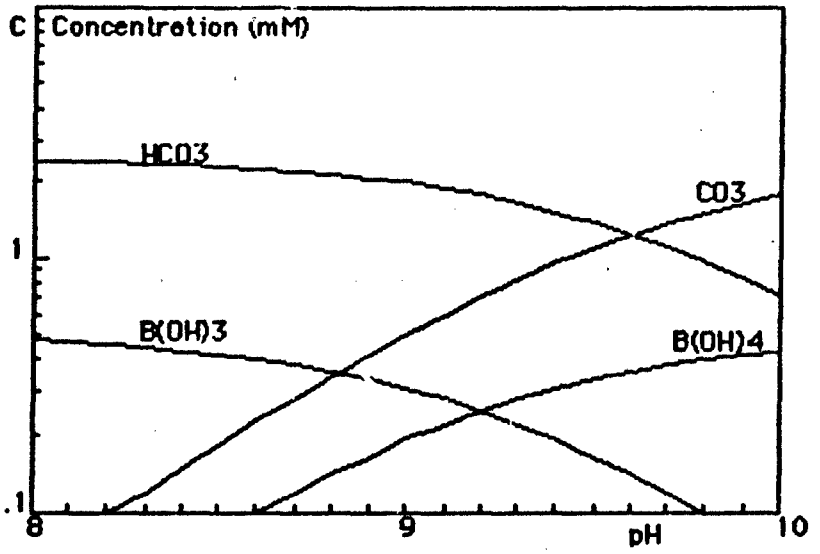

Figure 9: $B(OH)_3$ and CO_2 specie concentrations vs pH.

The proposed ionization equilibrium in sea water is given by:

$$B(OH)_3 + CO_3^{2-} + H_2O \leftrightarrow B(OH)_4^- + HCO_3^-$$

For chemical purposes, the individual equilibria can be written:

$$HCO_3^- \leftrightarrow H^+ + CO_3^{2-} \qquad K_C=[H^+][CO_3^{2-}]/[HCO_3^-]$$

$$B(OH)_3 + H_2O \leftrightarrow H^+ + B(OH)_4^- \qquad K_B=[H^+][B(OH)_4^-]/[B(OH)_3]$$

where $[H^+]$ is the hydrogen ion concentration and $pH=-\log([H^+])$. The equilibrium constants in these terms are $pK_B \approx 9.2$ and $pK_C \approx 9.8$.

Concentration of the carbonate ion, for example, is given by the formula:

$$[CO_3^{2-}] \approx [CO_2]\, 10^X/(1+10^X) \qquad X=pH-pK_C$$

where $[CO_2]$ is the total carbon dioxide concentration.

Possible effects of ion-pairing of carbonate with metallic ions were also pointed out. Carbonate has a strong affinity with sodium, magnesium and calcium ions. Bicarbonate affinities are much smaller and can be ignored. The principal equilibria to be considered are therefore:

$$Na^+ + CO_3^{2-} \leftrightarrow NaCO_3^- \qquad K \approx 1.6/M$$

$$Mg^{2+} + CO_3^{2-} \leftrightarrow MgCO_3 \qquad K \approx 53/M$$

$$Ca^{2+} + CO_3^{2-} \leftrightarrow CaCO_3 \qquad K \approx 125/M$$

In sea water, most of the carbonate exists in associated form and the CO_3 curve of Figure 9 represents the total of the four carbonate species.

Borate ion formulae are similar but the affinities are much smaller. Boric acid and bicarbonate affinities are negligible.

Sea-Data Analysis

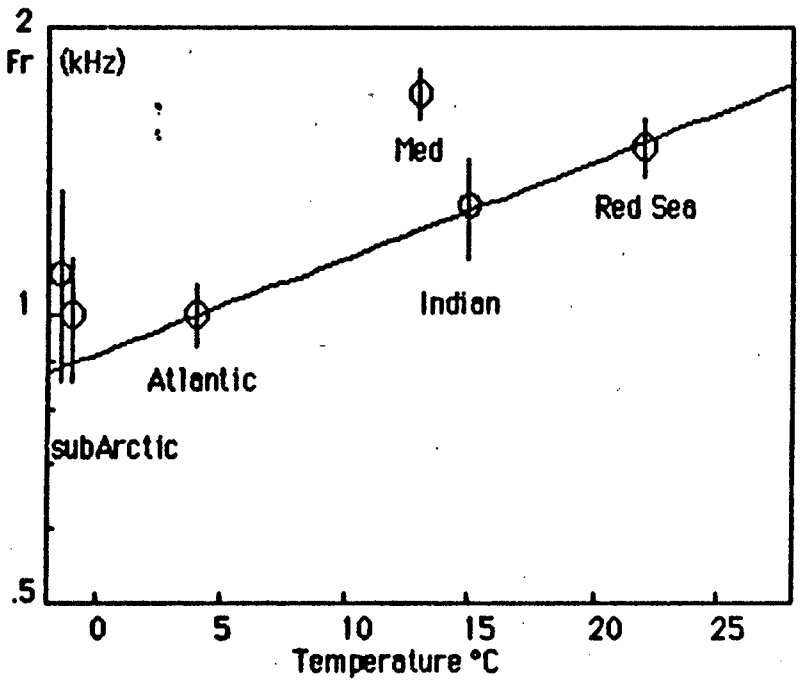

Figure 10: $B(OH)_3$ relaxation frequency data.

In order to estimate the relaxation frequency of boric acid with the two-component model, the measured absorption spectra had to be fitted by a curve with two other parameters; namely, the magnesium sulfate and boric acid coefficients. Because of limited accuracy of the low-frequency data, the boric acid relaxation frequency often tends to be difficult to determine with the required accuracy.

Figure 10 includes only those experiments for which reasonably good estimates of relaxation frequency could be obtained from analysis of the experimental data. The Atlantic and Red Sea experiments were believed to be the most accurate and were heavily weighted. The solid line is given by $f_r=0.9\times10^{T/100}$ (kHz), which intersects both points. In the analysis of the other data, this formula was taken to be the best estimate of relaxation frequency vs temperature at that time.

Except for Leroy's Mediterranean point, there is reasonable agreement within the limits of estimated experimental error. Further investigations have resolved all of the discrepencies, as will be seen in the later sections of this paper.

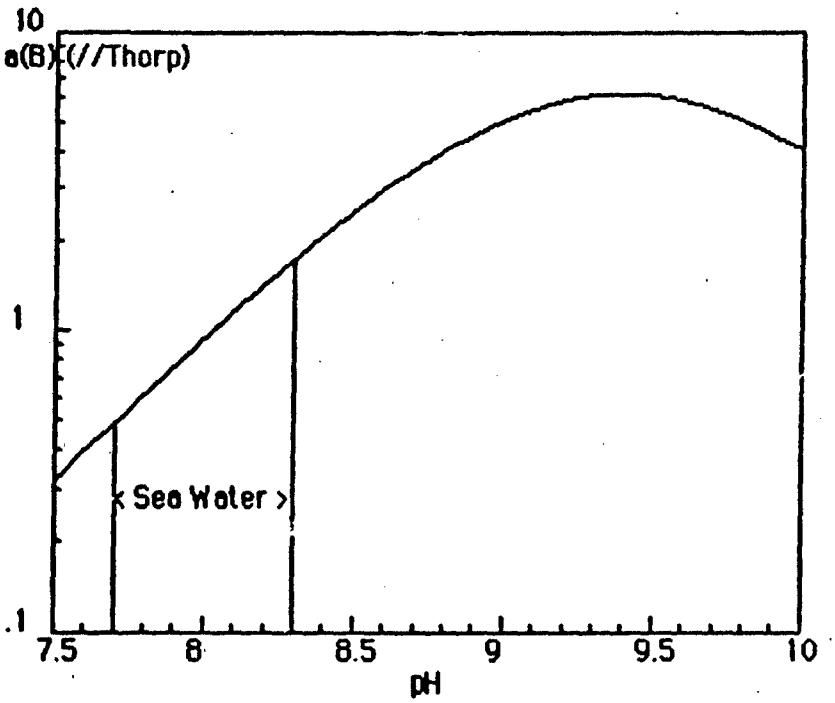

Figure 11: Boric acid coefficient a(B)//Thorp vs pH.

For the exchange mechanism proposed by Yeager et. al., the boric acid coefficient a(B) is proportional to the product of the two reactants on either side of the equilibrium as indicated earlier. Taking boric acid and carbonate as the reactants we have:

$$[B(OH)_3][CO_3^{2-}] \approx [B][CO_2]\ 10^x/(1+10^x)(1+10^y)$$

where [B] is total boric acid concentration and $x=pH-pK_C$, $y=pH-pK_B$

The coefficient should therefore increase exponentially and then decay after reaching a maximum value near pH≈9.5. In the curve Figure 11, the coefficient is expressed relative to Thorp's value. In the sea-water pH range, the coefficient increases approximately as 10^{pH}. In practice, pH>8.5 is not possible in sea water because calcium carbonate will precipitate out of solution.

The pH dependence of the experimental sea-data was investigated [14]. Analysis was based on the assumption that the rate constant, which controls the relaxation frequency, is the main temperature-dependent factor. The relaxation amplitude parameter, a(B), is easily determined when the relaxation frequency is calculated from the data-fit of Figure 10. The value should also be nearly independent of temperature because the rate constant then cancels out of the equation.

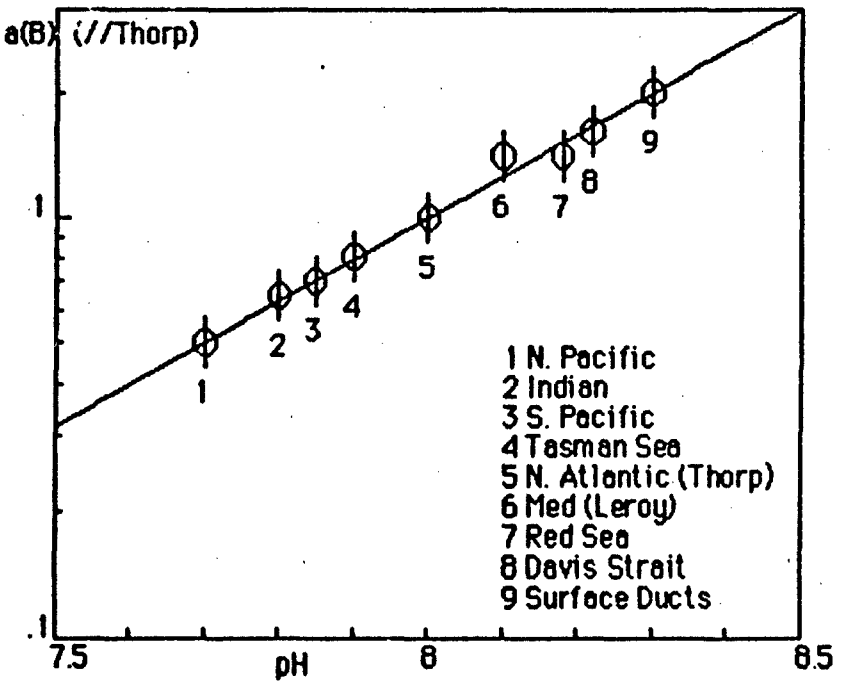

Figure 12: $B(OH)_3$ parameter a(B)//Thorp vs pH

All sea data were fitted by the two-relaxation model [14]. Values for the magnesium sulfate component were obtained by matching the spectra at the higher frequencies. Other components of low-frequency loss were also added when indicated. (see the later sections on diffraction and scattering loss). The parameters of the boric acid spectrum were then determined by adjusting the amplitude and relaxation-frequency parameters for "best-fit".

When the relaxation frequency could not be estimated with sufficient accuracy, the boric acid coefficient $A_{max}=a(B)\ f_r$ was measured The value of a(B) was then obtained by dividing A_{max} by the appropriate relaxation frequency from the data-fit of Figure 10. The values shown in Figure 12 are relative to Thorp's value a(B)=0.11, which is still believed to be the best approximation for the two-relaxation model.

The standard deviation of the data vs pH shows a correlation of better than 90% and no temperature trend is evident, supporting the assumption that relaxation frequency is the only temperature-dependent parameter. Using Thorp's pH=8 as the standard, the approximation for the absorption parameter becomes $a(B)=0.11\times10^{(pH-8)}$

Resonator Measurements

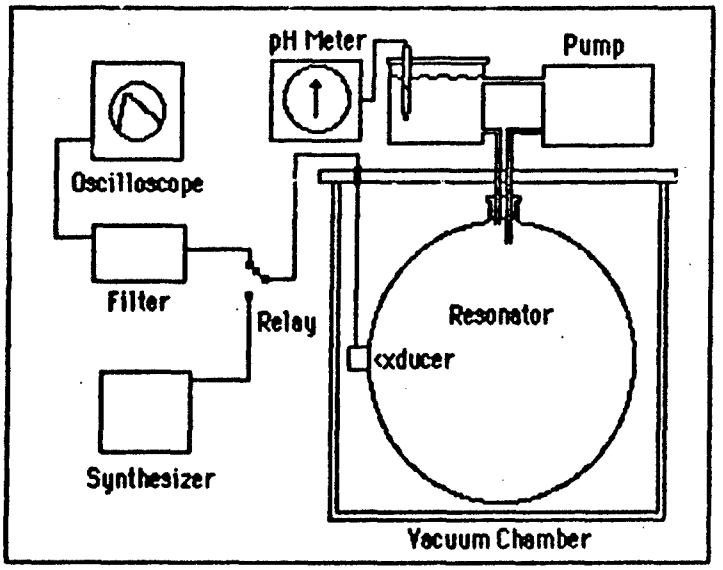

Figure 13: Resonator apparatus (ref. 16)

The temperature-jump measurements showed that only boric acid can produce a relaxation in the 1 kHz range. However, since the method permits measurement of relaxation frequency and not absorption, it was not yet clear what part it played in the actual absorption mechanism.

Resonator measurements in the 1 kHz range are not feasible because of size limitations. Subsequent investigations by Simmons [15], using the resonator method at higher frequencies and the temperature-jump method, proved that boric acid is essential to the low-frequency sound-absorption process. However, since aqueous boric acid showed comparable relaxation frequency as well as absorption, the mechanism remained uncertain.

From 1979-1983, resonator measurements of synthetic sea water (SSW) were carried out at NUSC by Mellen et. al. [16]. The apparatus is shown in Figure 13. The useable frequency band was limited to 10-100 kHz and the errors were estimated to increase from ±0.2 to ±1 dB/km in this range.

In order to measure the relaxation parameters, the reactions had to be maneuvered into the measurement window by increasing concentrations. Sea-water relaxation parameters were obtained by extrapolating back to normal concentrations. Sulfate was omitted in order to eliminate the magnesium sulfate relaxation and thereby improve the accuracy. Other relaxations involving magnesium were also discovered; however, of these, only the magnesium carbonate relaxation plays any significant role in sea water [16]. All relaxations were measured separately and in combination to determine interaction effects between them.

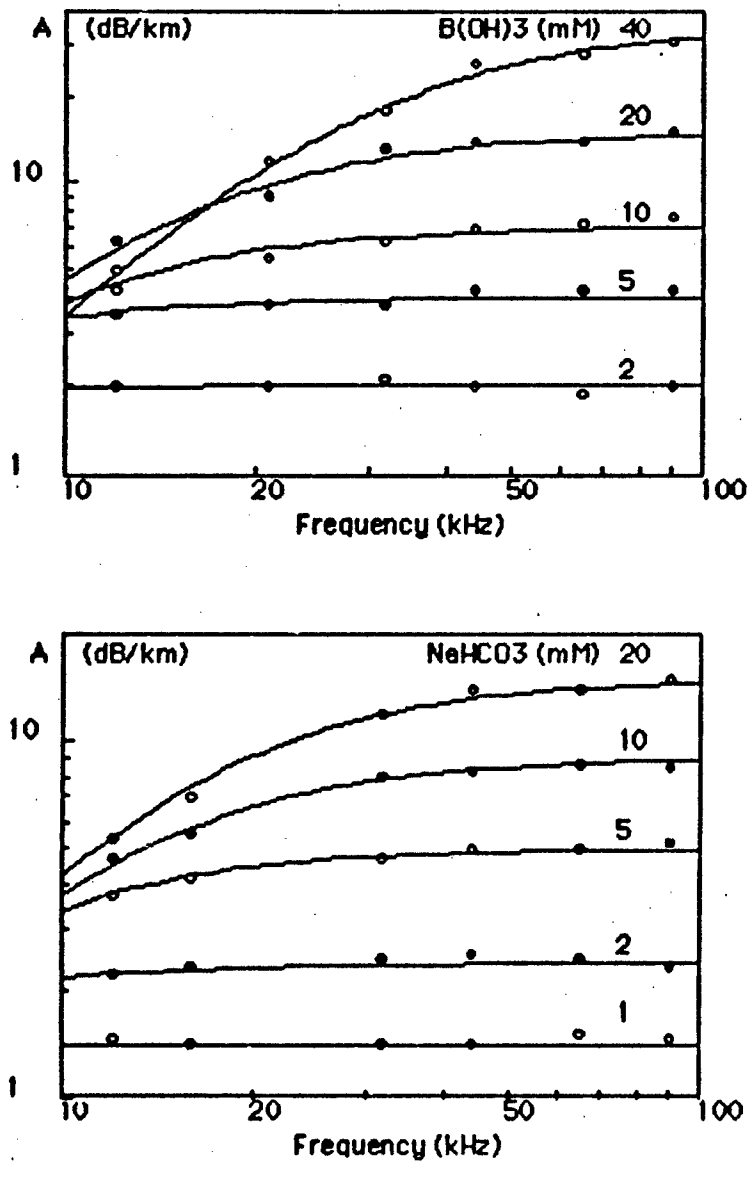

Figure 14: Boric acid absorption spectra at pH≈9.

Magnesium chloride has negligible effect on the boric acid relaxation and was omitted in the experiments of Figure 14 in order to eliminate the undesired relaxations. In the top spectra, calcium chloride was included at 10 mM and the sodium bicarbonate concentration was reduced to 1 mM in order to prevent precipitation of calcium carbonate. Relaxation frequency increases linearly with boric acid concentration to nearly 35 kHz. The lower spectra (calcium chloride omitted) show the same effects when the sodium bicarbonate concentration is increased and the concentration of boric acid is held constant (2 mM), confirming the exchange mechanism.

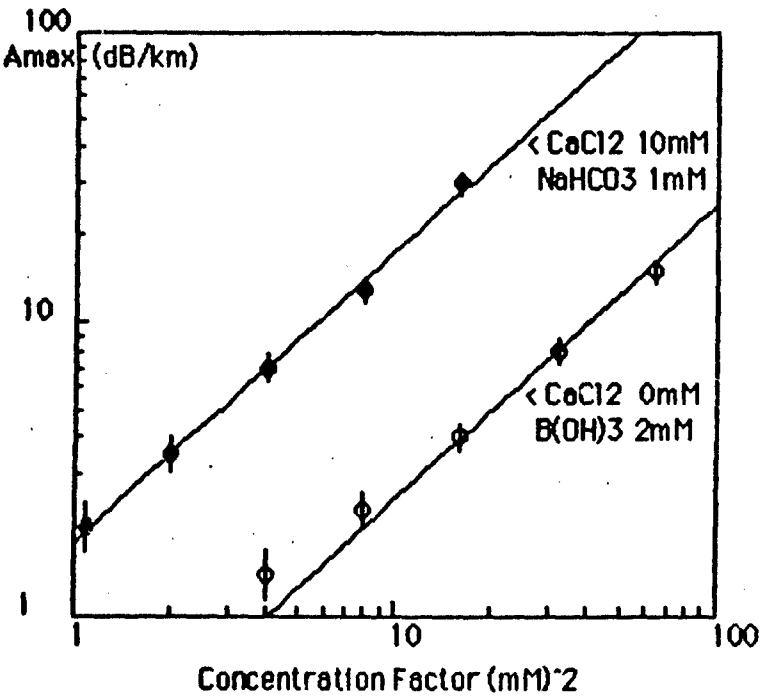

Figure 15: Boric acid Amax data vs concentration.

In figure 15, the maximum values of each spectrum of Figure 14 are plotted vs the relative concentration of the varied constituent.

Amax is proportional to the product of the reactants. The concentration factors $(mM)^2$ for the two cases are given by:

$$[B(OH)_3] \times [CO_{3\,tot}]_{const.}$$

$$[CO_3^{2-}] \times [B(OH)_3]_{const.}$$

With pH≈9 held constant, the concentration of the varied reactant is simply a constant factor times its total concentration. The calcium carbonate ion-pair concentration is included in the first case. Calcium chloride was omitted in the second case.

Both data sets are proportional to the concentration factor; however, the absorption increases dramatically when calcium is included, which clearly indicates a large contribution to ΔV. The other metallic ions do not show any significant effects.

Extrapolated to sea-water concentrations and pH, the data with calcium are in good agreement with sea measurements. Without calcium, the values are too low by almost an order of magnitude.

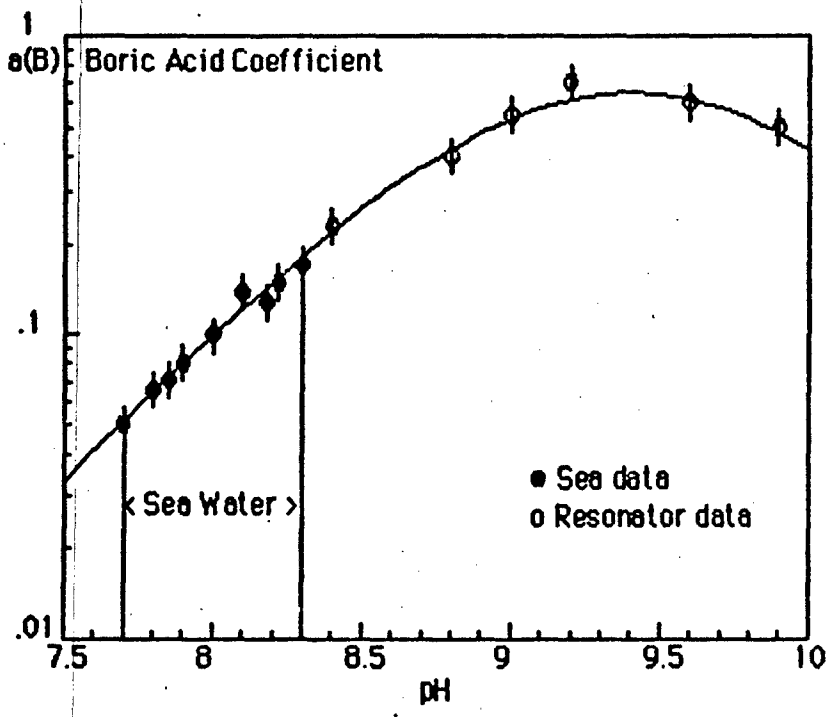

Figure 16: Comparison of resonator and sea data vs pH.

Figure 16 shows a comparison of the boric acid resonator data with the sea data of Figure 12. The resonator data were obtained at elevated boric acid concentrations and were corrected to sea-water concentration by extrapolation.

The resonator experiments confirm, in detail, that the boric/carbonate exchange is the dominant mechanism and that all assumptions are valid.

As the result of this work, it is believed that the boric acid absorption mechanism is now understood to almost the same degree as that of magnesium sulfate. However, to construct an practical absorption model based solely on relaxation chemistry would be far too complex and the accuracy would be limited to that of the supporting measurements as well. Therefore, the combined results of resonator, T-jump and sea experiments have been taken into consideration in the development of a simplified model for the boric-acid mechanism.

There are a number of possible models for the boric acid/carbonate equilibrium in sea water. One that is both tractable and consistent with the experimental data is preferred as a matter of convenience and may not represent all the essential chemical details involved.

Boric Acid Mechanism

$$B(OH)_3 + CaCO_3 + H_2O \leftrightarrow B(OH)_4^- + HCO_3^- + Ca^{2+}$$

principal exchange reaction

$$B(OH)_3 + CO_3^{2-} + Ca^{2+} + H_2O \overset{1}{\leftrightarrow} B(OH)_4^- + HCO_3^- + Ca^{2+}$$

$$\updownarrow 3 \qquad\qquad \updownarrow 4$$

$$B(OH)_3 + CaCO_3 + H_2O \overset{2}{\leftrightarrow} CaB(OH)_4^+ + HCO_3^-$$

coupled exchange reaction

$$fr \approx \frac{k'}{2\pi}\left([B(OH)_3] + [HCO_3^-]/K_1\right) \quad (Hz)$$

$$A_{max} \approx \frac{(\Delta V)^2 k' [B(OH)_3][CO_{3\,tot}]\rho c^2}{2R(T+273)} \quad (Np/sec)$$

absorption formula parameters

$\Delta V \approx -22$ ml/mole

$k' \approx 4 \times 10^{6+T/70}$ /mol*sec

R=gas constant T=temp °C

ρ =density c=sound speed

$K_1 = K_B/K_{2C} \approx 4$

Figure 17: Boric acid relaxation equilibria.

The top box of Figure 17 shows the principal equilibrium describing the essential chemical factors involved. However, the relaxation frequency for this model depends on calcium concentration, which is not observed experimentally.

The second box shows details of the proposed ion-pair equilibria. In this case, the two sides are separated by equally slow steps and relaxation frequency is quite independent of calcium concentration. This model is used as the basis of the present analysis.

Simplified formulae for the absorption parameters for the model are given in the third box. Species having negligible effect on relaxation frequency are omitted in the formula.

The bottom box shows the estimated values of the relaxation parameters ΔV, k' and K_1.

Other Relaxations

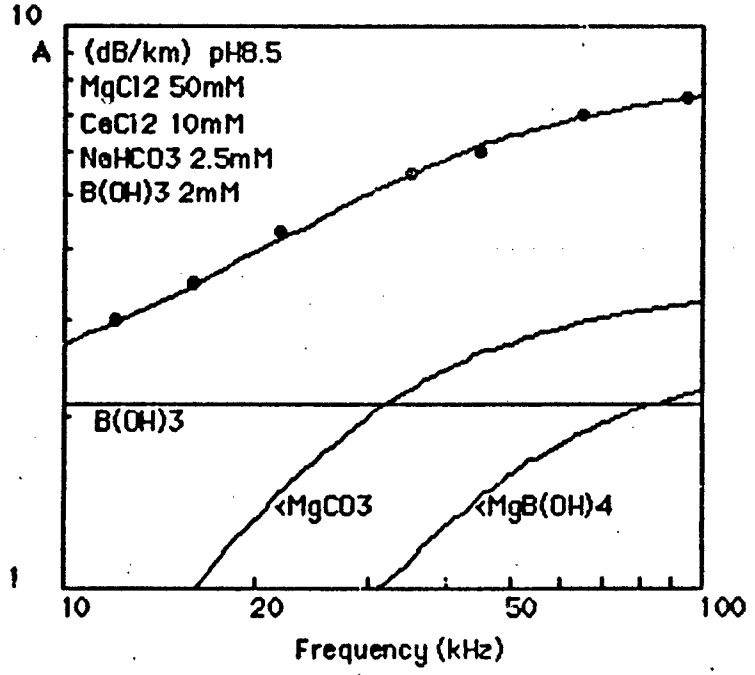

Figure 18. Absorption spectra of $B(OH)_3/CO_2/Mg/Ca$ system.

The contributions of two other relaxations involving magnesium are shown in Figure 18. The mechanisms of both appear to be similar to magnesium sulfate and are modeled by two-step equilibria:

$$(MgCO_3)_I \leftrightarrow (MgCO_3)_{II} \leftrightarrow Mg^{2+} + CO_3^{2-}$$

$$(MgB(OH)_4^+)_I \leftrightarrow (MgB(OH)_4^+)_{II} \leftrightarrow Mg^{2+} + B(OH)_4^-$$

Both relaxations have been studied independently. In the magnesium carbonate experiments, boric acid was omitted. In the magnesium borate experiments, sodium bicarbonate was omitted. Without carbonate, boric acid absorption is so small that it can be ignored.

Temperature, concentration and pH dependencies of both relaxations were determined from the relaxation spectra.

With the parameters of the two relaxations known, the two systems were then combined to determine any interaction effects. The results shown in Figure 18 indicate that interactions are negligible and that all three components are simply additive.

For normal sea-water boric acid concentration, the magnesium borate component becomes negligible. The magnesium carbonate component, while small, can become significant at high pH values [17].

Absorption Model

$$A = A_1(MgSO_4) + A_2(B(OH)_3) + A_3(MgCO_3)$$

$$A_n = a_n f^2 f_n / (f^2 + f_n^2)$$

$$a_1 = 0.5 \times 10^{-d(km)/20} \qquad f_1 = 50 \times 10^{T/60}$$

$$a_2 = 0.1 \times 10^{(pH-8)} \qquad f_2 = 0.9 \times 10^{T/70}$$

$$a_3 = 0.03 \times 10^{(pH-8)} \qquad f_3 = 4.5 \times 10^{T/30}$$

Atlantic 4°C pH 8.0 $A = 0.007f^2 + 0.1f^2/(1+f^2) + 0.18f^2/(6^2+f^2)$
N.Pacific 4°C pH 7.7 $A = 0.007f^2 + 0.05f^2/(1+f^2) + 0.09f^2/(6^2+f^2)$
Mediterranean 14°C pH 8.3 $A = 0.006f^2 + 0.26f^2/(1.4^2+f^2) + 0.78f^2/(12^2+f^2)$
Red Sea 22°C pH 8.2 $A = 0.004f^2 + 0.27f^2/(1.8^2+f^2) + 1.1f^2/(24^2+f^2)$
sub-Arctic -1°C pH 8.3 $A = 0.01f^2 + 0.17f^2/(0.85^2+f^2) + 0.24f^2/(4^2+f^2)$

Figure 19: Simplified absorption formulae.

The simplified formula for the 3-relaxation model is shown at the top of Figure 19 where A is the absorption coefficient (dB/km), f is frequency (kHz), T is temperature (°C) and pH=8.0 is the reference value. The pure-water term is omitted, making the formula valid for frequencies less than roughly 100 kHz. The pressure factor in the magnesium sulfate formula of Fisher and Simmons [18] for has been modified as the depth term D(km) in this model. Depth dependencies of the other relaxations are not yet known; however, measurements in both deep and shallow channels indicate that the effect on boric acid must be very small. Magnesium carbonate effects may be greater but can be neglected because its contribution is so small. Salinity dependence is neglected temporarily but will be considered in a later section.

Specific values for several experimental locations are also shown in the bottom box. Note that the magnesium sulfate terms A1 are approximations valid only for $f \ll f_1$.

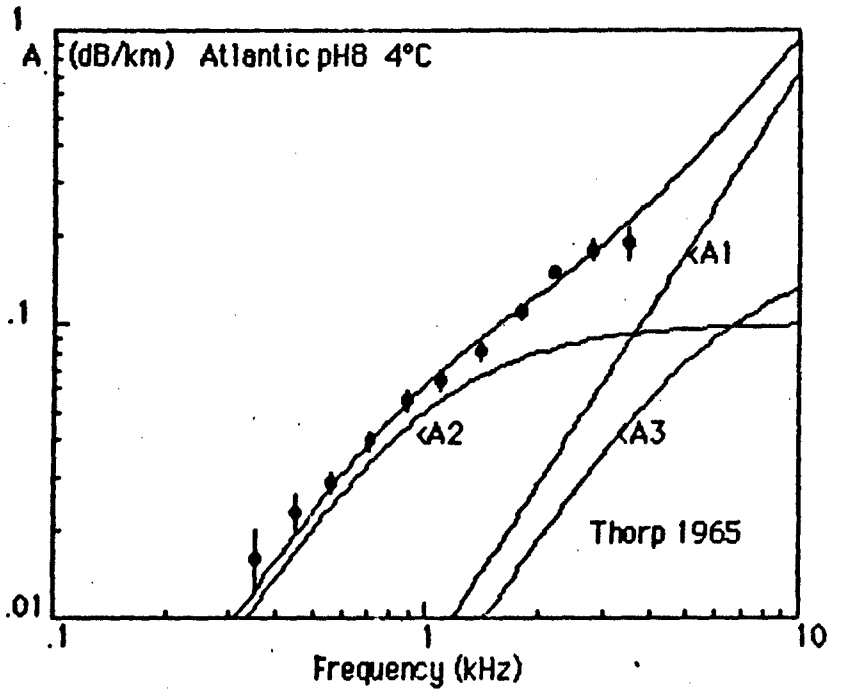

Figure 20: Thorp's data and model.

Figure 20 shows Thorp's data compared to the 3-component relaxation model. Note that the magnesium sulfate (A1) coefficient is 0.007 rather than the earlier value 0.009 used in the 2-component model. The new value is based on a very careful laboratory re-evaluation of magnesium sulfate absorption in sea water by Fisher and Simmons [18].

Note also, that the boric acid (A2) coefficient is 0.1 compared to 0.11 in the 2-component model. The magnesium carbonate (A3) component makes up for both differences and the fit to the data is somewhat better.

The possible existence of a third relaxation in sea water was proposed earlier by Fisher [19]. He observed a persistent bump in the data around 3-4 kHz that could not be removed by any consistent readjustment of the parameters of the 2-component model. The discovery of the magnesium carbonate relaxation in Lake Tanganyika and subsequent study of the mechanism put the hypothesis on very firm ground. In fact, resonator measurements of sea water at pH≈8.5 revealed, beyond all doubt, the deficiencies of the 2-component model. Regardless of any reasonable readjustment of the parameters, measured values were much too high without the third component [17].

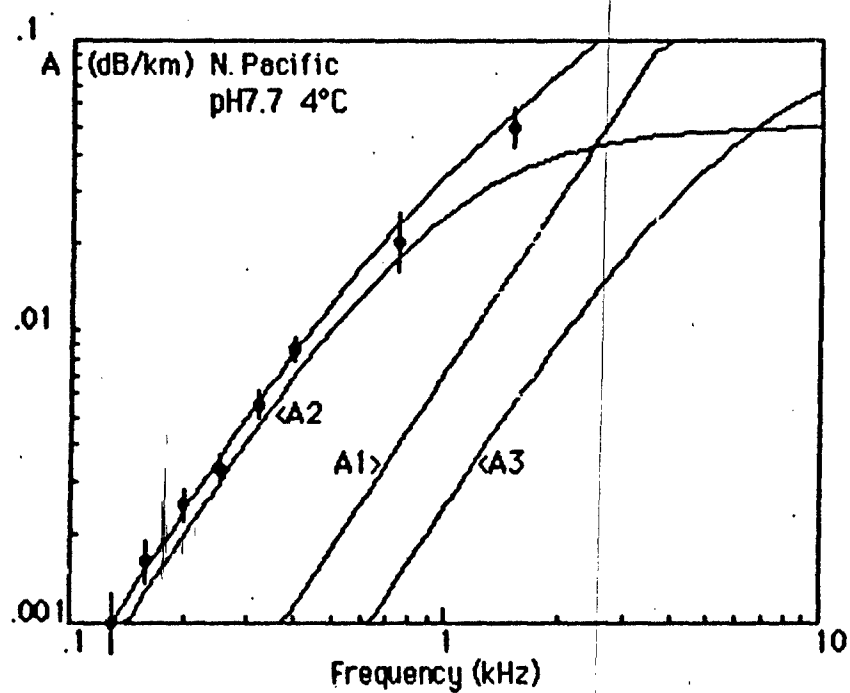

Figure 21: North Pacific data and model.

In the North Pacific model, the lower value pH≈7.7 reduces both the boric acid (A2) and the magnesium carbonate (A3) coefficients by a factor of two compared to Thorp. Relaxation frequency depends only on temperature and remains the same. Note that the dB/km scale has been reduced by the factor 10 in Figure 21.

Sea water is highly alkaline. Values of pH in the World Ocean range from about 7.7 to 8.3 whereas the neutral value is 7. Surface values average around 8.1 and tend to have a much narrower range. Evidently, circulation and contact with the atmosphere are involved in controlling pH. The lowest values are found in deep waters where the circulation times are the longest, which would account for the very low absorption observed in the North Pacific sound-channel.

At the higher latitudes, the sound-channel axis comes to the surface as the thermocline diminishes and the absorption increases because the pH is higher. The very low-absorption phenomenon is therefore probably limited only to the central North Pacific Ocean.

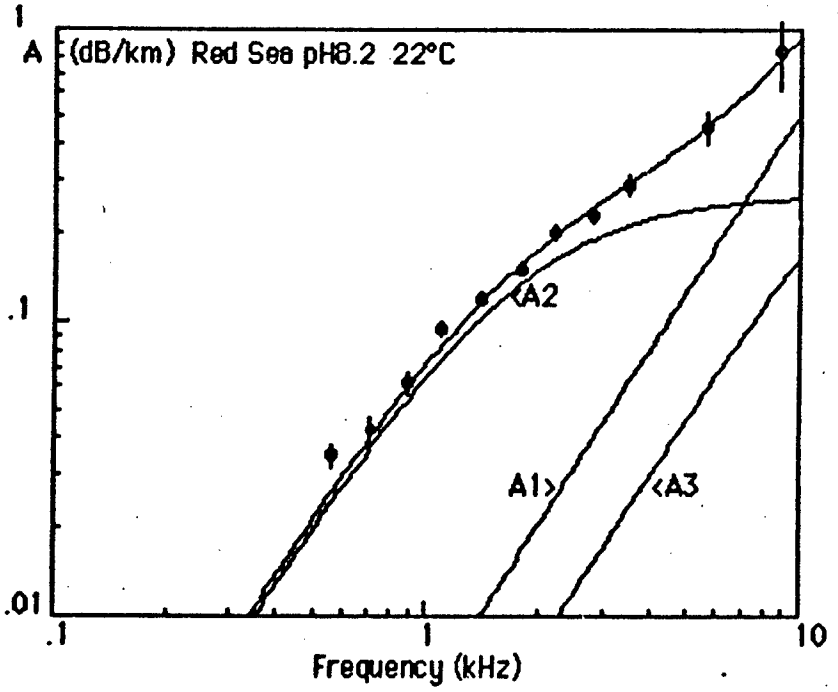

Figure 22: Red Sea data and model.

The Red Sea data were originally fitted with a 2-relaxation model and the results indicated a low-frequency relaxation at 1.5 kHz compared to the formula value 1.8 kHz. Figure 22 shows that an even better fit is achieved with the 3-relaxation model using the latter value.

The major remaining anomaly appears to be the 1.7 kHz relaxation frequency of Leroy's Mediterranean experiment. Since the method of measurement is different, other sources of error must be considered.

Experiments reported here made use of explosive sources. A possible source of error is nonlinearity wherein the overtaking effect regenerates some of the lost high-frequency energy at the expense of low. Earlier, an attempt was made to explain the entire attenuation anomaly by such a mechanism. However, propagation in a sound channel involves phase shifts at caustics, which reverses nonlinear effects so that there is negligible accumulation at long ranges. Leroy's ranges were limited to the first convergence; i.e.≈40 km. If the wavefront remains coherent over the entire propagation path, effects can be significant.

The recent Mediterranean sound-channel experiment appears to support this argument because the range extended to more than 600 km and results are consistent with the model.

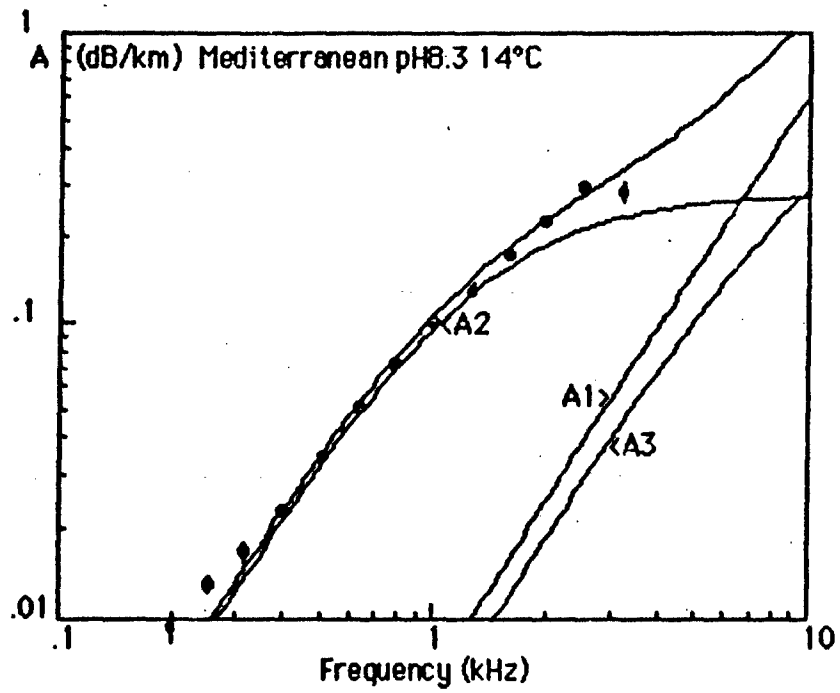

Figure 23: Mediterranean data and model.

The Mediterranean experiment was carried out in the deep Ionian basin between Sicily and Crete in July 1982 by SACLANTCEN [1]. Sound velocity profiles indicated a strong sound channel with a rather broad minimum at 100-200 m depth. Temperature, salinity and sound-speed profiles were uniform over the 640 km path. Effects of the rising bottom were noted only at extreme ranges and these points were omitted in the analysis.

Measurements of pH and boric acid concentrations also showed little variability with range or depth over the track. The high pH value is typical of surface values in other regions. Both the boric acid and carbon dioxide concentrations were found to be normal. The salinity (S≈38) is slightly higher than normal.

At pH=8.3, the boric acid coefficient is a factor of 2 greater than that for the North Atlantic. However, the much higher temperature increases the relaxation frequency so that the absorption spectrum is not increased by such a large factor at the lower frequencies.

The 3-component relaxations calculated for the experimental conditions are shown in Figure 23 and the fit to the data is clearly excellent.

Diffraction Effects

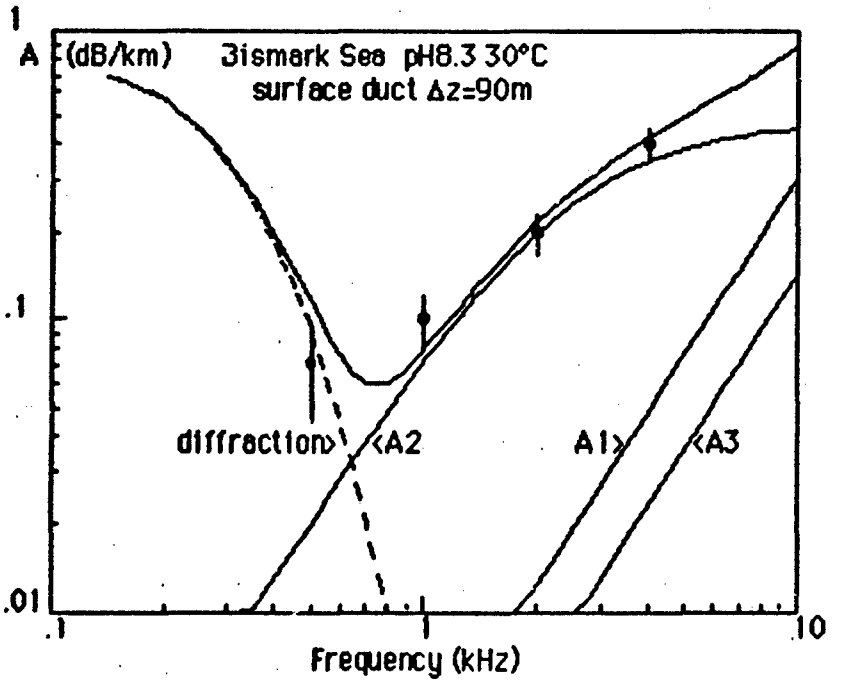

Figure 24: Bismark Sea surface-duct data and model.

An experiment in the Bismark Sea by Wylie [20] indicates the need for including diffraction loss in surface-duct calculations. In this case, the duct depth was approximately 90m. Diffraction effects become significant when the acoustic wavelength becomes too large for total refractive trapping. The consequence is an additional component of attenuation that increases rapidly with decreasing frequency.

Acoustic trapping is the result of an isothermal mixed-layer at the surface overlying the thermocline. The sound-speed gradient in the layer can be approximated as that in deeper isothermal water. The diffraction loss in Figure 24 was calculated for a bilinear gradient with the normal positive gradient down to the duct depth and a negative gradient of larger magnitude below. Note that trapping is never total; however, the loss decreases exponentially with increasing frequency and rapidly becomes negligible. The only effect of diffraction, in this case, appears to be the absence of data at frequencies below effective cutoff.

The absorption model was calculated for the ambient temperature 30°C and the pH=8.3 was estimated from archival data. Agreement with the data above 1 kHz indicates that surface scattering was negligible as expected for the low sea state.

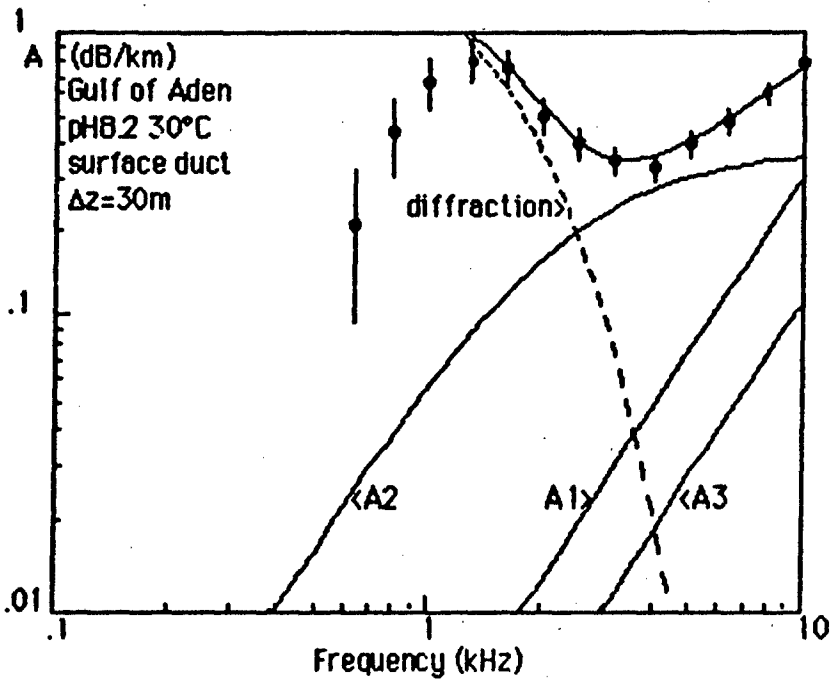

Figure 25: Gulf of Aden surface-duct data and model.

In the Gulf of Aden experiment [12], the duct depth was only 30m and the calculated diffraction effect remains strong to well above 1 kHz. However, the data shows increasing attenuation over only a limited range and the trend reverses as frequency decreases. This is the result of the leaky surface-duct signals returning from the deep channel.

The absorption model was calculated for the ambient temperature 30°C and the pH value estimated from archival data. Agreement with the data above 1 kHz indicates plausibility of both the absorption and diffraction models.

Sea states in both experiments were very low and the absence of surface loss was not unexpected. In most sound-channel experiments, refractive trapping by the thermocline tends to make effects of surface scattering negligible. However, if the thermocline is weak or absent, the excess loss should certainly become appreciable at moderate sea states. In such cases, a marked frequency-dependence is expected, particularly at the lower frequencies. For acoustic wavelengths large compared to the surface wavelength, the excess loss should fall off very rapidly.

Lake Experiments

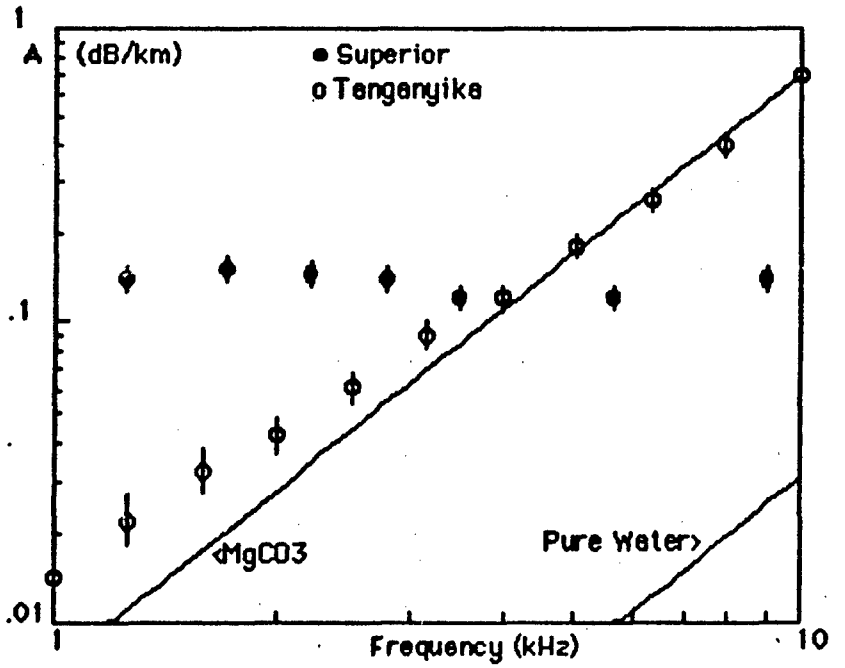

Figure 26: Lake experiments.

The experimental program of Browning et. al. [12] included two lake experiments for comparison purposes. Both gave surprisingly anomalous results compared to pure water as seen in Figure 26.

Attenuation in Lake Tanganyika was found comparable to the magnesium sulfate relaxation in sea water. Analysis of the constituents showed that the concentration was too low by a factor of 30 to account for the result; however, both the carbon dioxide content and pH≈8.5 were abnormally high. Chemical synthesis of artificial lake water in other resonator experiments showed the mechanism to be the magnesium carbonate relaxation.

Attenuation in Lake Superior of was found to be comparable to that of boric acid in sea water. In this case, the anomaly has been attributed to internal scattering. Frequency-independent attenuation is apparently the result of multiple-scattering by large-scale temperature inhomogeneities within the thermocline. Energy gradually diffuses out of the channel by a "random-walk" process and is absorbed in the bottom. This mechanism seems to be common to all sound-channel experiments; however, it is usually observed only at very low frequencies [21]. Much of the spread in scattering loss can be attributed to differences in channel strength; however, no reliable method of prediction has yet been found.

Scattering Effects

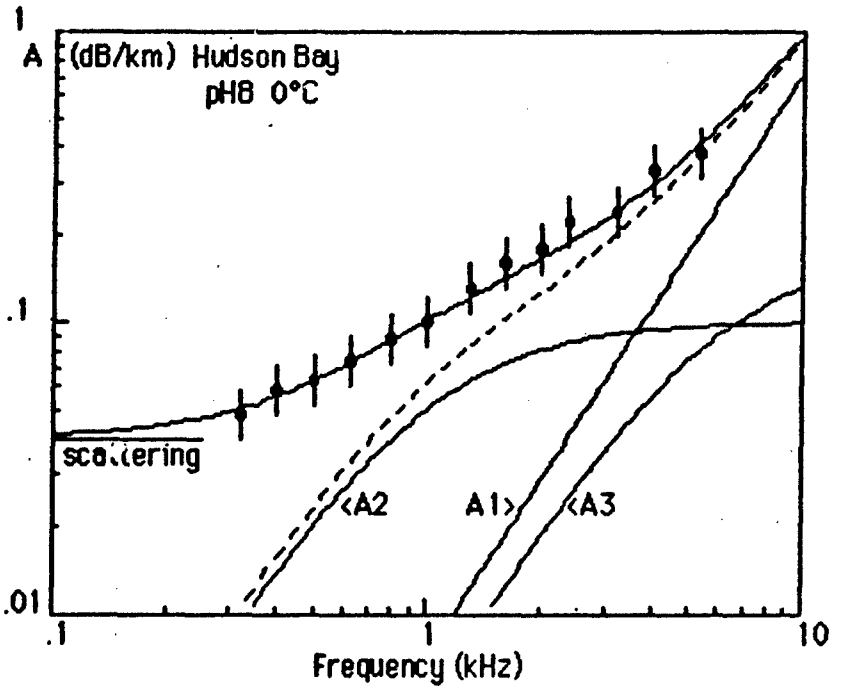

Figure 27: Hudson Bay data and model.

Hudson Bay [12] was the first sea experiment to show excess frequency-independent loss and served to put the scattering hypothesis on more firm footing. The puzzling result of the earlier Lake Superior experiment, in particular, was clearly attributable to the same mechanism.

Since the loss is independent of frequency, ray-diffusion theory will be applicable and losses can be calculated from the diffusion equation [21]. Diffusion loss depends inversely on the strength of the channel. In order to reach the bottom, axial rays must overcome a potential barrier ΔC, which is the difference in sound-speed between the bottom and channel axis. For small angles, loss is inversely proportional to the square of the critical angle of the bottom-grazing ray.

In Figure 27, the dashed line is the estimated total absorption, and the excess scattering-loss is taken as 0.04 dB/km independent of frequency. Water depth in Hudson Bay is only 100m and trapping is weak. Although the Lake Superior depth is nearly the same, a slight negative temperature-gradient reduces the channel strength, making the loss approximately four times greater.

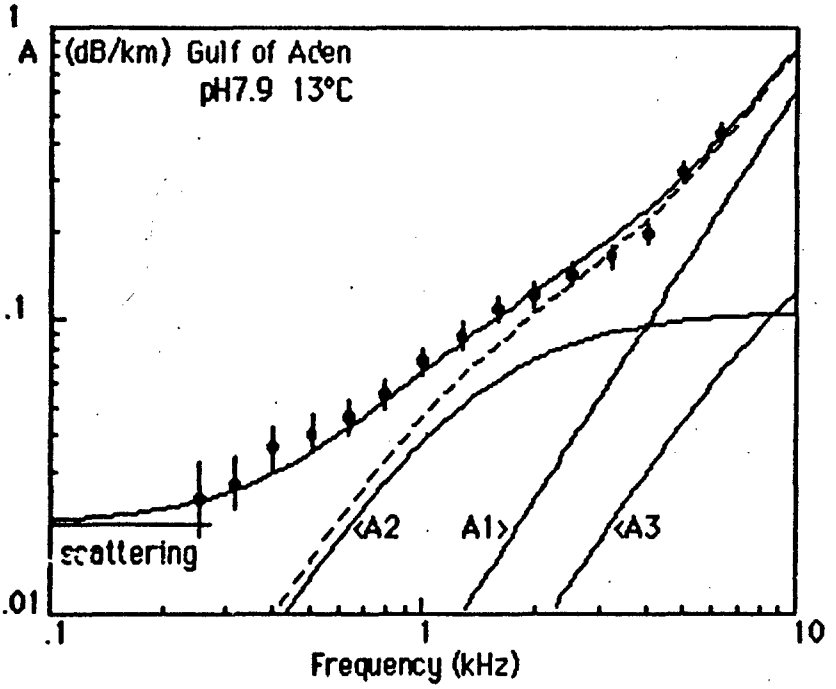

Figure 28: Gulf of Aden data and model.

In the Gulf of Aden experiment [12], there was a strong intermediate sound channel caused by outflow of water from the Red Sea. This is in addition to a deeper channel and the surface duct discussed earlier. Source and receiver were located in the intermediate channel. The experimental track was 500 km in length and the total water depth was roughly 1 km. Absorption parameters are estimated for the ambient temperature 13°C and archival value pH=7.9 at axis depth.

Despite the relatively strong trapping in the intermediate channel, there is marked evidence of scattering loss. This may be the result of instability in the upper part of the thermocline where the temperature falls from 30°C at the surface to 20°C at 100 m. Sound-speed profiles indicated a great deal of fluctuating fine-structure and this could account for the reverse scattering back into the surface duct as noted in Figure 25. In addition, scattering into the deeper channel may also be a significant factor.

In Figure 28, an additional component of 0.02 dB/km has been added to fit the data.

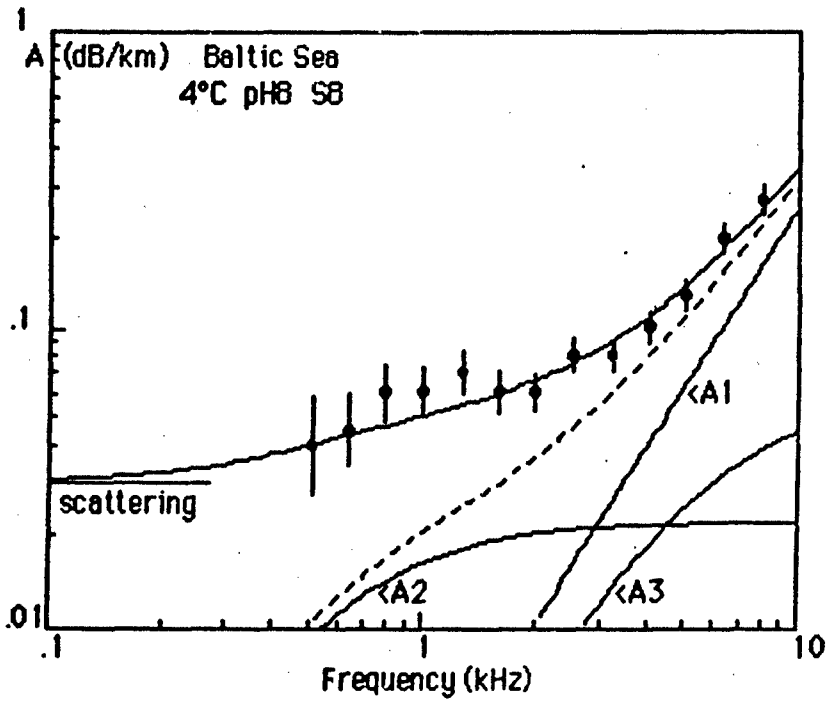

Figure 29: Baltic Sea data and model.

Interpretation of attenuation measurements in the Baltic Sea [22] indicates need for estimating sound absorption in low-salinity waters.

While the magnesium sulfate component depends simply on the first power of concentration, the low-frequency boric acid relaxation is more complex. The mechanism involves exchange with carbonate in which the ion-pair calcium carbonate governs the absorption magnitude.

Measurements of absorption by the resonator method show roughly 1/2 power dependence on calcium concentration in the range of interest.

The Baltic Sea salinity of 8 is about 25% normal while the carbonate and acidity are both normal. Since loss is multiplicative, $S^{1.5}$ dependence is indicated. This would yield a reduction in magnitude by the factor 8. However, a more exact calculation, taking into account the coupled-ion effects, shows somewhat less reduction. In addition, relaxation frequency is lower. T-jump measurements of Baltic water samples by Candau [23] (unpublished) show that it is only 0.6 kHz, which agrees with theory. All factors have been included in the calculations.

Comparison of the measured data in Figure 29 shows that attenuation is still anomalously high by a large factor. The relative weckness of the lower part of the channel due to the small water-depth (≈100 m), is again indicatative of loss by internal scattering.

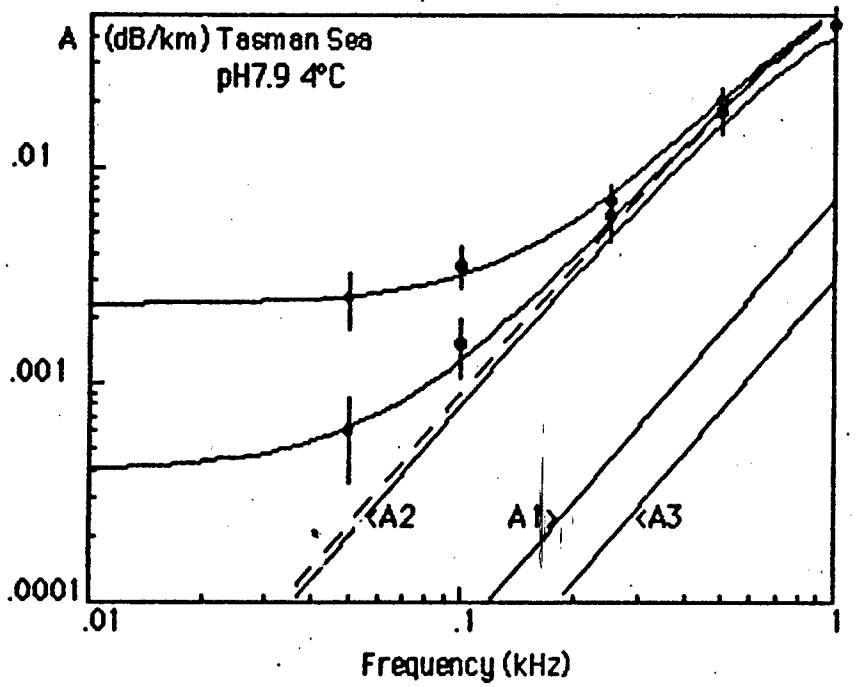

Figure 30: Tasman Sea data and model.

In the deep ocean, the sound-channel is much stronger and scattering loss ranges from negligible to only a few dB per thousand kilometers. The measurements in the Tasman Sea by Bannister et. al. [24] in Figure 30 are typical. In both experiments shown, measurements were made in the deep channel and the maximum range was roughly 3000 km. The absorption spectrum was calculated for pH=7.9, a value estimated from archival data.

In the lower curve, a scattering loss of 3×10^{-4} dB/km has been added in the data-fit. This amounts to only 1 dB total over the path and is probably insignificant. In the upper data, the scattering loss is taken as 2×10^{-3} dB/km and amounts to roughly 6 dB total, which is considered well beyond the limits of experimental error.

In the top experiment, the track encountered the Sub-Antarctic Front where the channel axis rises close to the surface. Range dependence of the sound-speed profile may account for some of the anomaly; however, the absence of frequency dependence of suggests that internal scattering is again the principal mechanism.

Regional dependence of scattering loss has also been investigated in the North Pacific by Kibblewhite et. al. [25]. Their results indicate a similar increase at higher latitudes that the range dependence of the sound-speed profile does not account for.

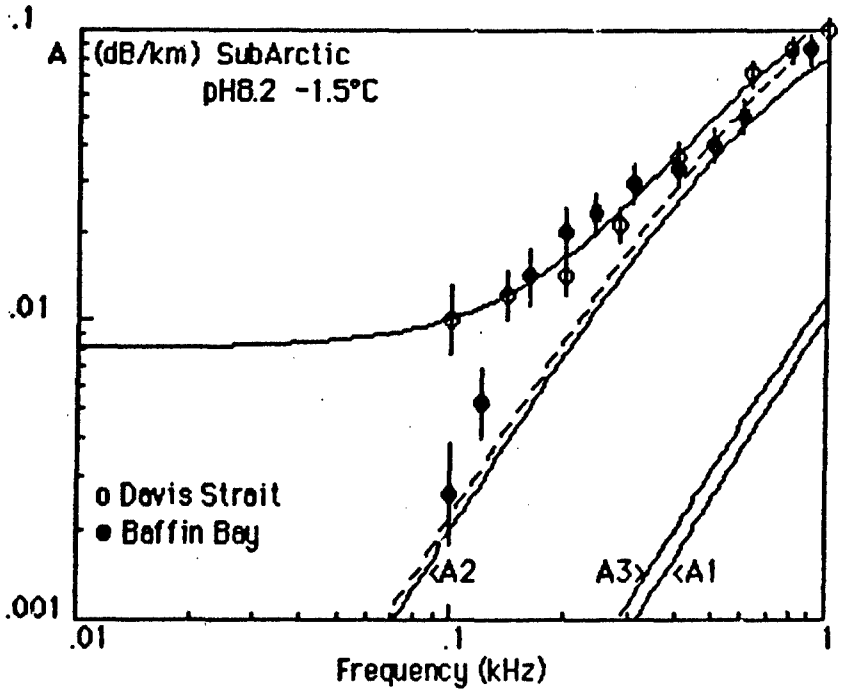

Figure 31: Sub-Arctic data and model.

Figure 31 shows results from two experiments by DREA in ice-free waters west of Greenland. Both of the tracks analyzed were in excess of 300 km in length with water depths of 1-2 km. The sound-speed profiles showed a distinct channel with axis depth near 100 m and any surface-scattering effects are therefore believed to be negligible. Absorption has been calculated for pH=8.2, which is consistent with archival data.

The southern track in the Davis Strait shows clear evidence of an excess scattering-loss component despite the strong channel. The data are fitted by adding the value 8×10^{-3} dB/km, which is comparable to the highest values reported in any of the experiments [25].

The northern track in Baffin Bay also shows a similar excess loss but only at the higher frequencies. At 100 Hz it becomes negligible. A possible explanation is that the bottom absorption at lower frequencies may be smaller in that area, causing energy to be reflected back into the channel. Alternatively, the inhomogeneities may be smaller in scale. Scattering loss can be expected to decay rapidly when the dimensions become small compared to the acoustic wavelength.

Model Summary

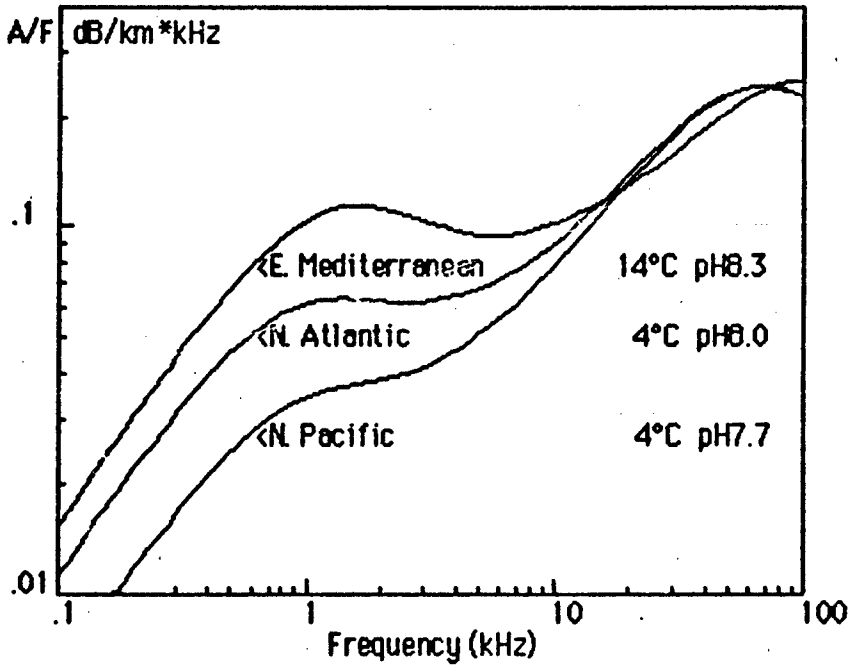

Figure 32: Experimental absorption spectra comparison.

The absorption spectra for the North Atlantic, North Pacific and Eastern Mediterranean experiments are compared in Figure 32. The coefficients have been divided by frequency in kHz in order to compress the scale.

The North Atlantic and North Pacific are apparently the extreme cases for deep (>1km) waters of the World Ocean. For latitudes less than 45°, the axis depth of the deep sound-channel is roughly 1 km; therefore, the two cases represent the limits of variability expected for sound-channel propagation in this latitude range. For the pH range 7.7-8.0, the max/min ratio increases uniformly with decreasing frequency, approaching a factor of two.

The Eastern Mediterranean is the highest pH so far; however, since the temperature is also high, the curve is displaced upward in frequency and the max/min ratio is slightly less than a factor of two compared to the North Atlantic.

From all the experimental evidence, it appears that the North Pacific and Eastern Mediterranean absorption spectra encompass nearly all the range of expected variability.

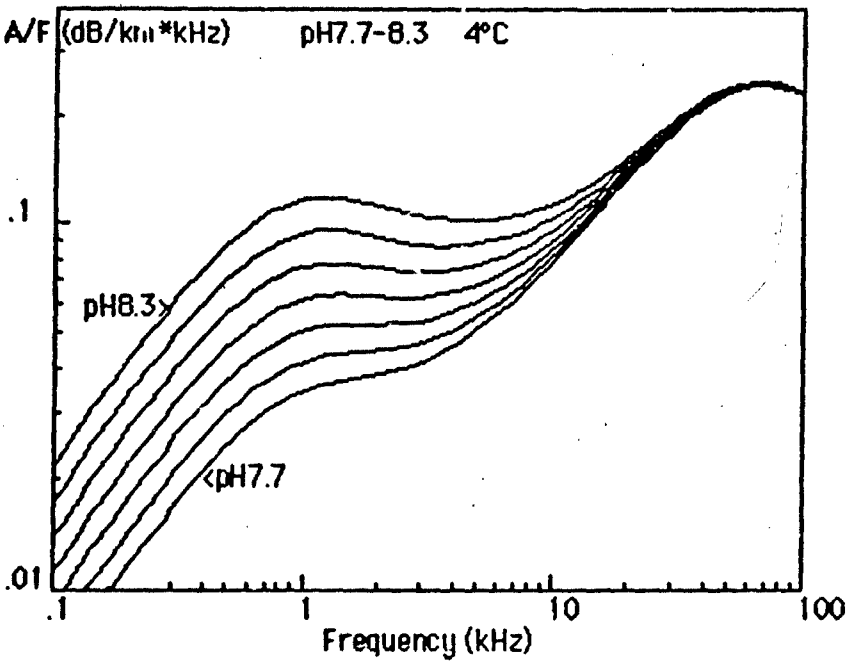

Figure 33: Absorption spectra A/F vs pH for T=4°C.

The principal results of the 3-relaxation model, are summarized in Figures 33 and 34. The absorption coefficient A has again been divided by the frequency in kHz in order to compress the range. The predicted spectra vs pH for 4°C and normal salinity (S=35) are shown in Figure 33 and cover the approximate sea-water range of pH 7.7-8.3 in steps of 0.1.

The effect of pH on the absorption spectrum below 10 kHz is mainly due to the coefficient of the boric acid component. Below 1 kHz, the max/min ratio approaches the factor four.

From the present analysis of the experimental data, the overall error of the absorption model is estimated to be roughly of the order of ±15%. In other words, the RMS error of an estimated coefficient in dB/km at any given frequency is not expected to be greater than this amount if not limited by the accuracy of the environmental factors. Since a change of 0.05 pH units corresponds to a 12% change in the boric acid coefficient, the pH errors must be within these limits in order to realize the model accuracy. The major limiting factor therefore appears to be the accuracy and availability of of the pH data-base.

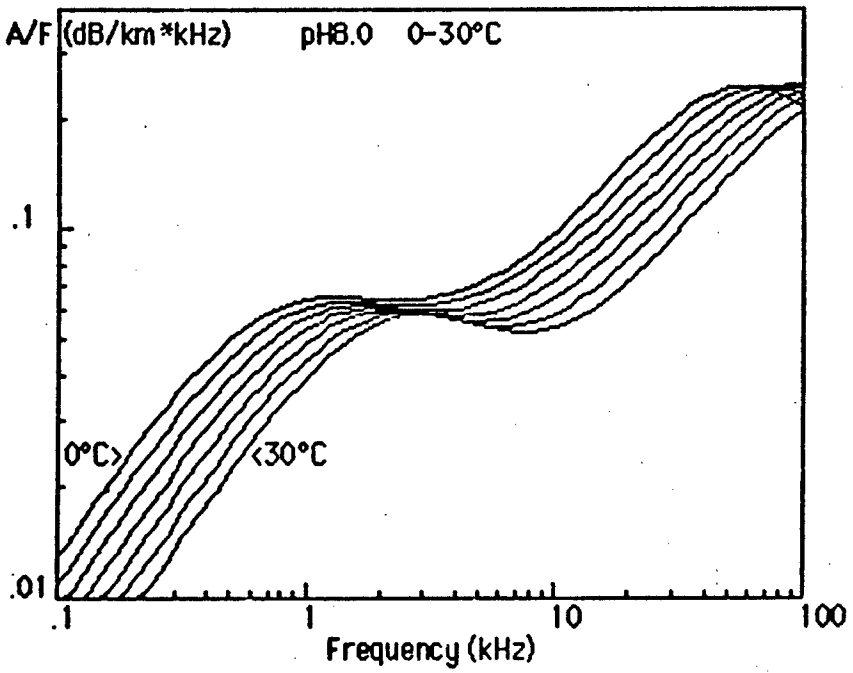

Figure 34: Absorption spectra A/F vs temperature for pH8.0.

Figure 34 shows the predicted spectral dependence on temperature for pH=8.0 and normal salinity (S=35) and cover the nominal sea-water range 0-30°C in 5°C steps.

The temperature effect in the model comes only through the relaxation frequency coefficients of all three terms. Increasing temperature shifts the curves upward in frequency.

Model errors involving temperature coefficient are also estimated to be of the order of ±15%. Since the temperature sensitivity is rather low, the value need only be known only to within roughly ±2°C to realize the same estimated accuracy.

Salinity corrections have been omitted in the simplified model. Errors are probably within the accuracy limits for the normal sea-water range 32-38 ppt. Salinity variations are evidently the result of evaporation and dilution by fresh water. Therefore, the concentrations of all constituents, except carbon dioxide, tend to remain in constant ratio. A multiplying factor S/35 for all three components may be justified over a limited range, say 30-40 ppt. Beyond this range, corrections must be made for changes in the boric acid relaxation frequency. In more extreme cases like the Baltic Sea, chemical analysis of the constituents may be required.

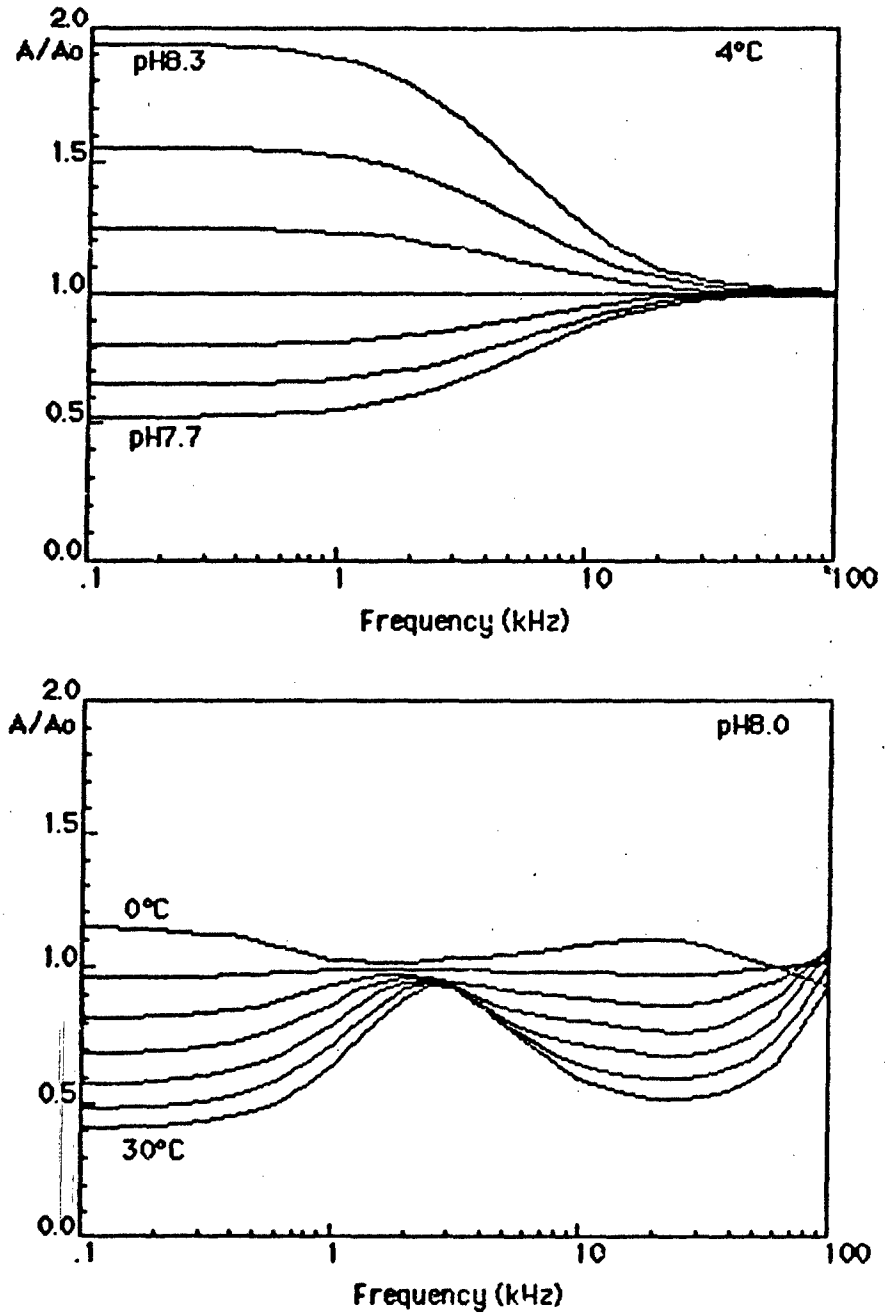

Figure 35: Absorption ratio A/Ao vs pH and temperature.

In Figure 35, the spectra of Figures 33 and 34 are expressed as the ratio A/Ao where the Ao is calculated for the North Atlantic parameter values pH=8.0 and T=4°C. The range of pH is 7.7-8.3 in steps of 0.1 and the range of temperature is 0-30°C in steps of 5°C. The curves indicate the accuracies required to realize the desired error limits.

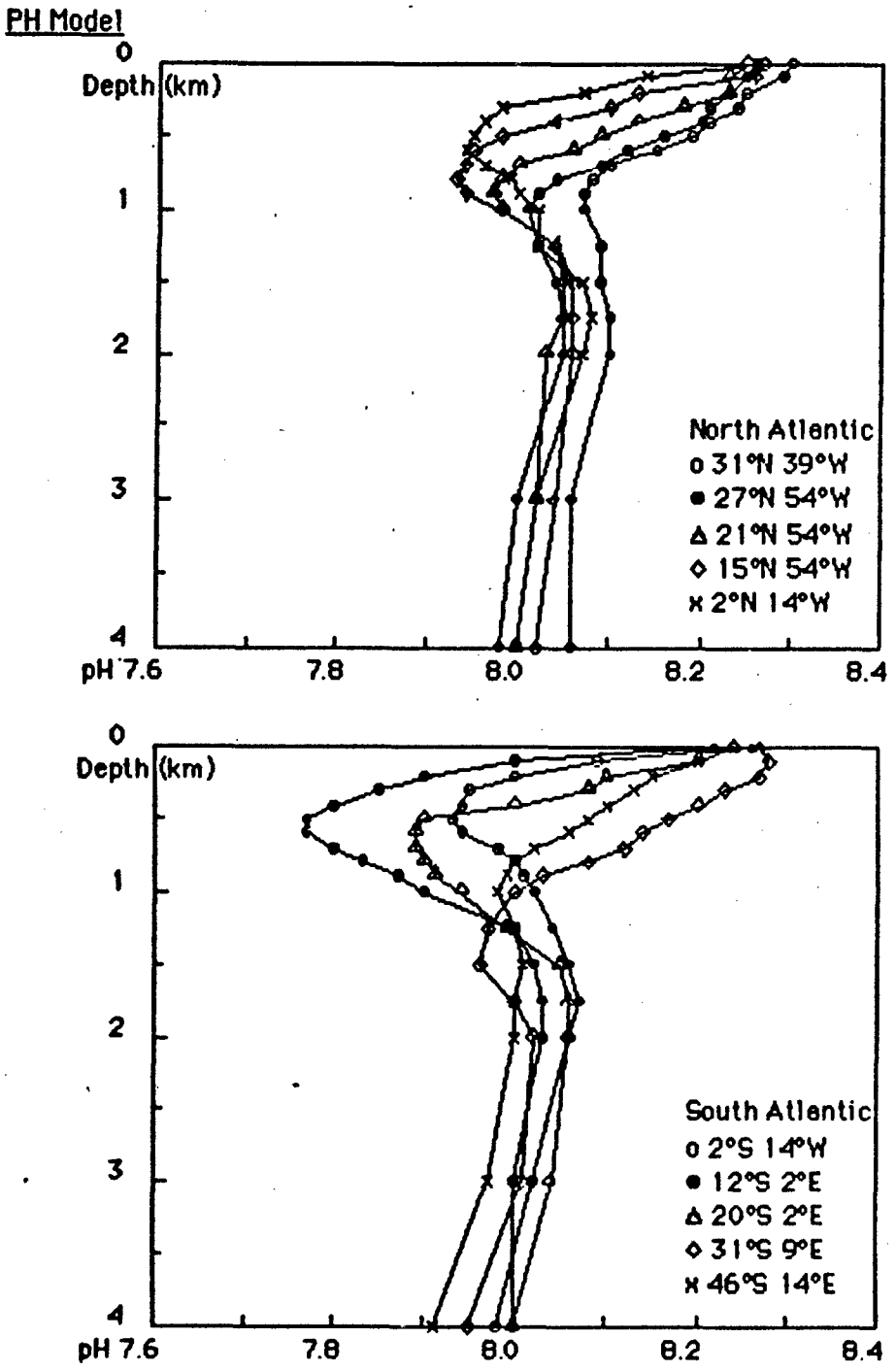

Figure 36: Atlantic Ocean pH profiles.

PH data for many regions of the World Ocean are included in the data of the GEOSECS oceanographic expedition report [26]. Figure 36 shows plots of typical profiles for a range of latitudes in the Atlantic Ocean.

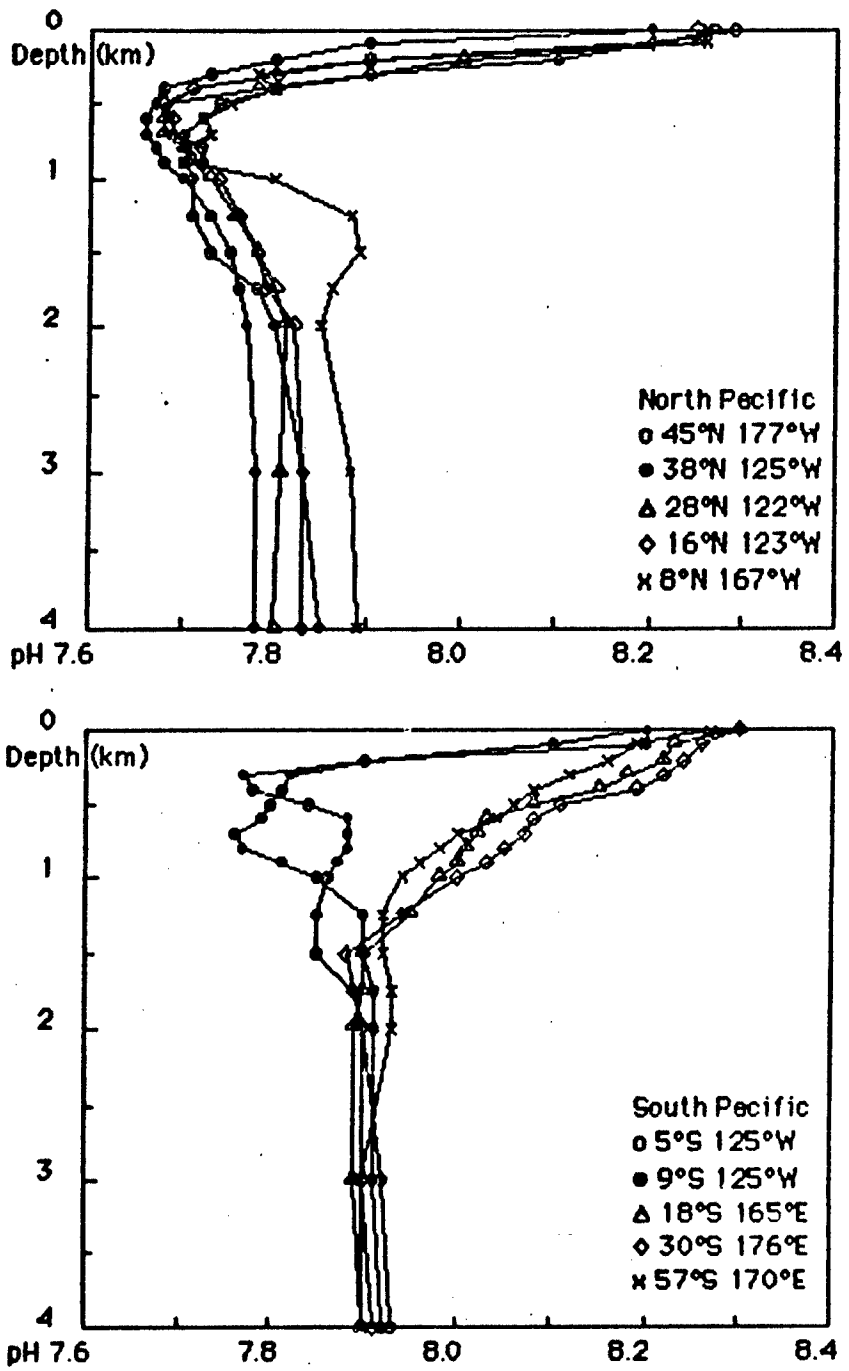

Figure 37: Pacific Ocean pH profiles.

Figure 37 shows plots of typical pH profiles for a range of latitudes in the Pacific Ocean from GEOSECS data [26].

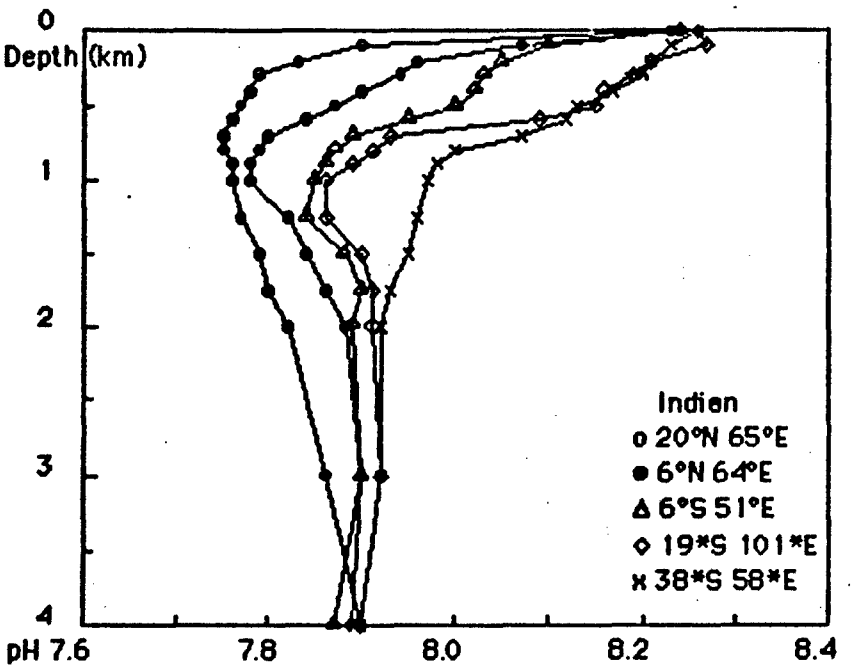

Figure 38: Indian Ocean pH profiles.

Figure 38 shows plots of typical pH profiles for a range of latitudes in the Indian Ocean from GEOSECS data [26].

A striking feature of all the pH profiles is the relative constancy of the values at the surface and at great depths. The greatest variability occurs in the thermocline region around 1 km. depth.

For surface-duct propagation, depth variability should be small because both the pH and temperature obviously are quite constant in the surface mixed-layer.

For convergence-zone propagation, most of the travel time is in the deep water where the pH is relatively constant. In the Southern Ocean, the value is 7.9. In the North Pacific, pH decreases to 7.8. In the North Atlantic, it increases to 8.1 at high latitudes. Variability with latitude can therefore be expected to be relatively easy to estimate.

The sound-channel axis depth is roughly 1 km at mid-latitudes and rises to the surface at high latitudes. The net result is that the pH value on the axis will tend to increase at the higher latitudes. The axial pH range is approximately 7.7-8.3 and values tend to vary rapidly and unpredictably with latitude. Sound-channel absorption should therefore be the most difficult to estimate with acceptable accuracy.

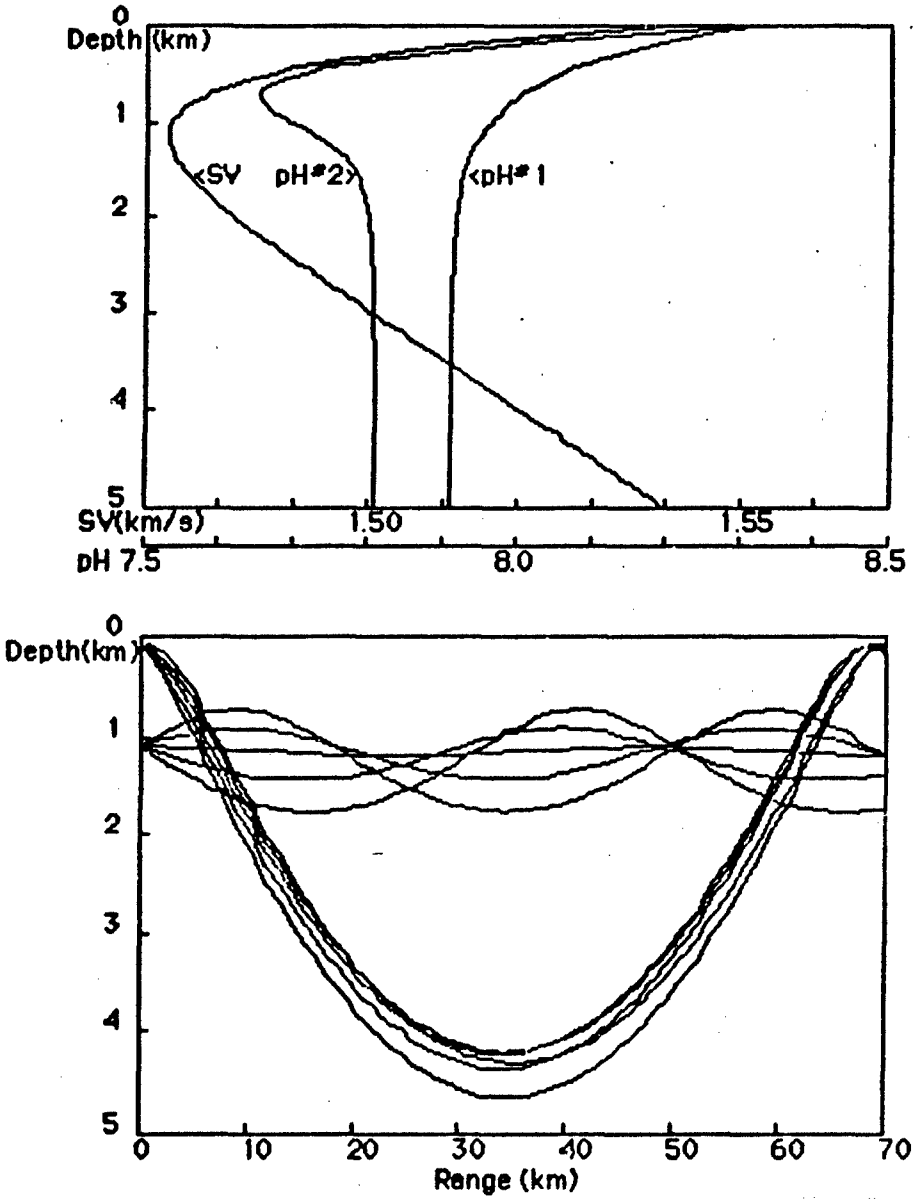

Figure 39: PH test profiles and ray paths.

In order to estimate the effects of the pH profiles at mid-latitudes, the two typical cases illustrated at the top of Figure 39 will be examined. The sound-velocity profile (SVP) is typical of latitudes less than 45°. Profile pH# 1 is the simple exponential decay and pH#2 is the case where there is a sharp minimum above the axis as in the North Pacific. Effective values of A for the two profiles are calculated by numerical integration of the loss over single cycles of the sound-channel and convergence-zone (CZ) ray paths shown at the bottom.

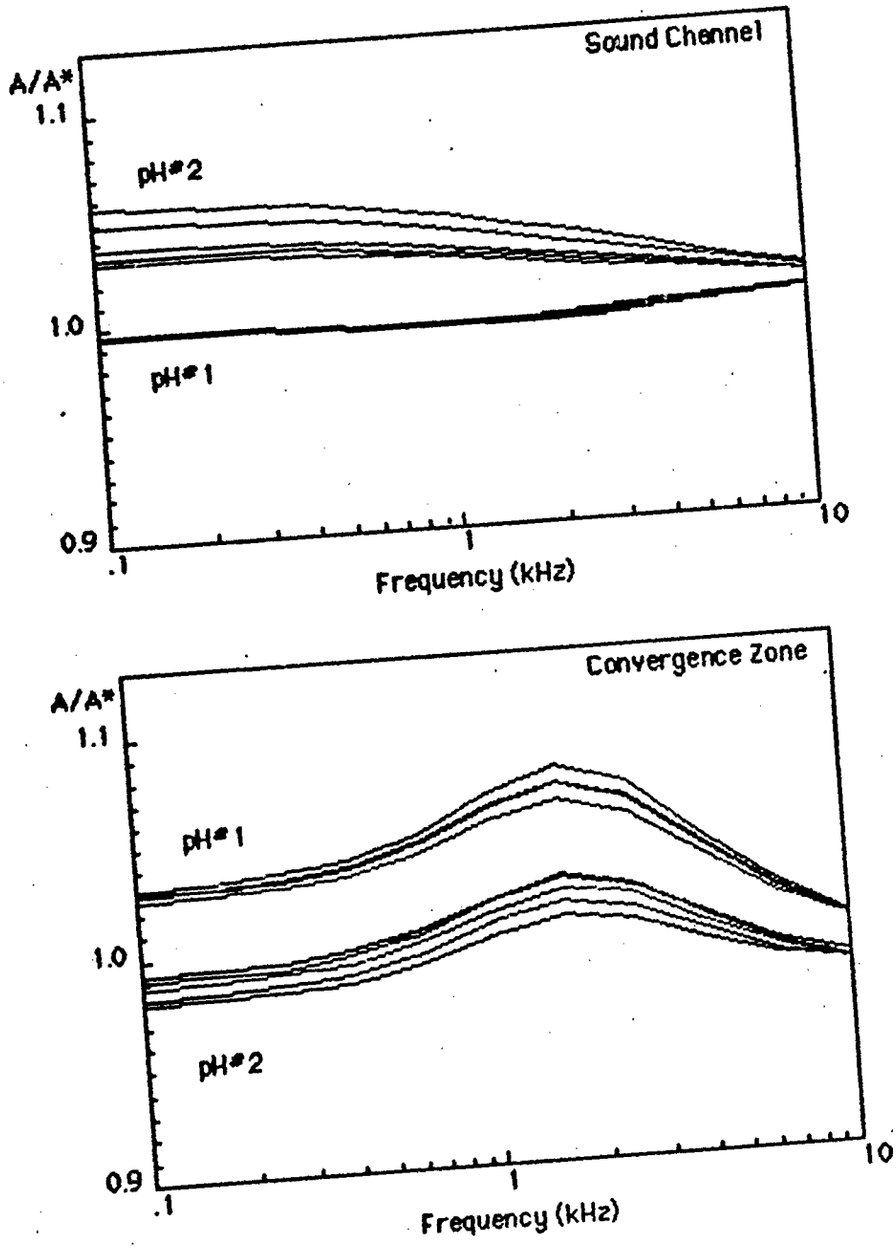

Figure 40: Absorption ratio A/A*.

Figure 40 shows the effective values of A relative to where A* is the value calculated using the axial temperature and pH for the sound-channel case and 2 km depth values for the CZ case. The results show that the net errors are far less than the estimated uncertainty in absolute pH values, which is taken to be ±0.05 units and corresponds to ±12% change in A/A*.

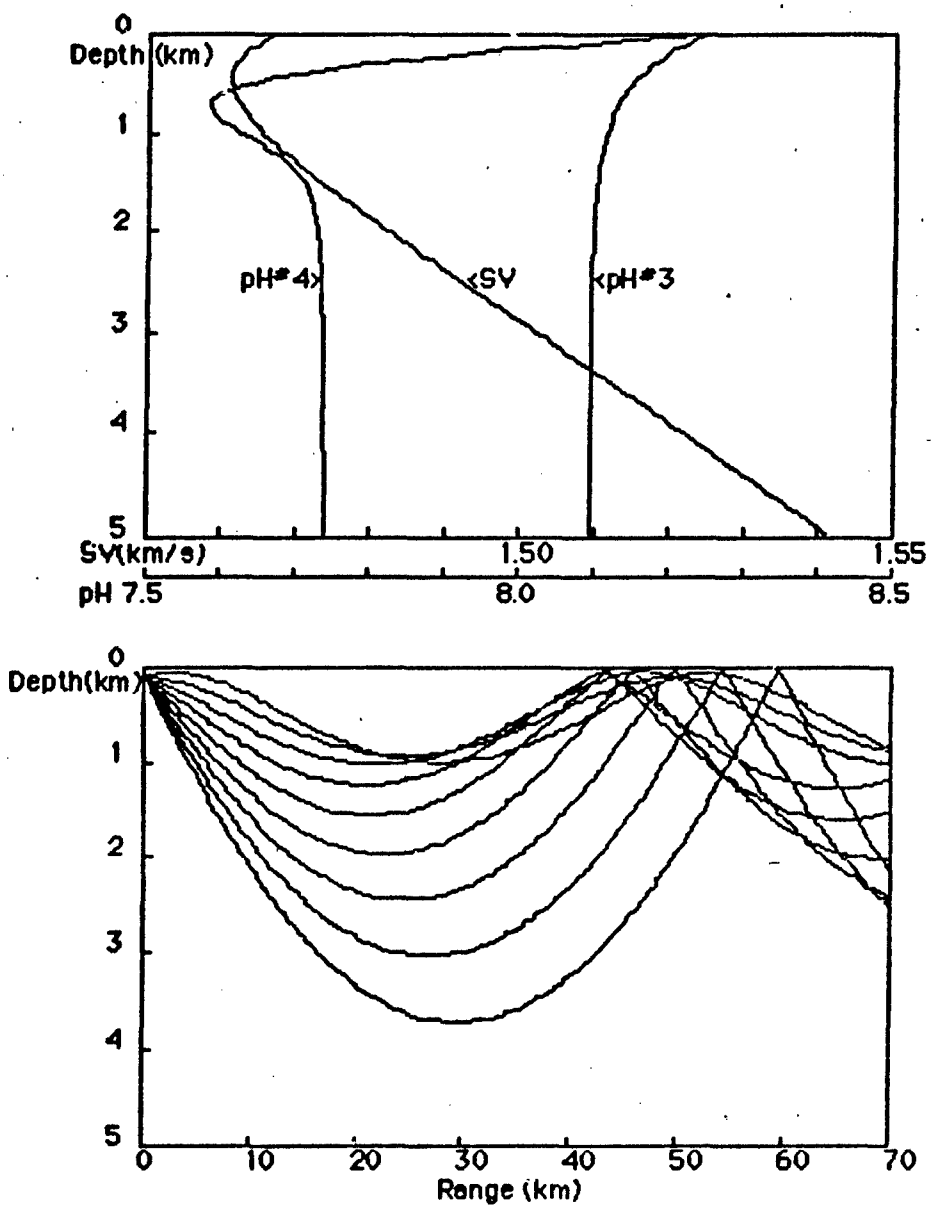

Figure 41: High latitude test profiles and ray paths.

In order to estimate effects of the pH profiles at higher latitudes, the two cases shown at the top of Figure 41 will be examined. The SVP is typical of latitudes around 60°. Profiles pH*3 and pH*4 represent current estimates for the North Atlantic and North Pacific, respectively. The ray paths used in the numerical integration of loss are shown below. Note the relative lack of distinction between sound-channel and convergence modes for shallow ray-angles. At higher angles, surface reflection is involved.

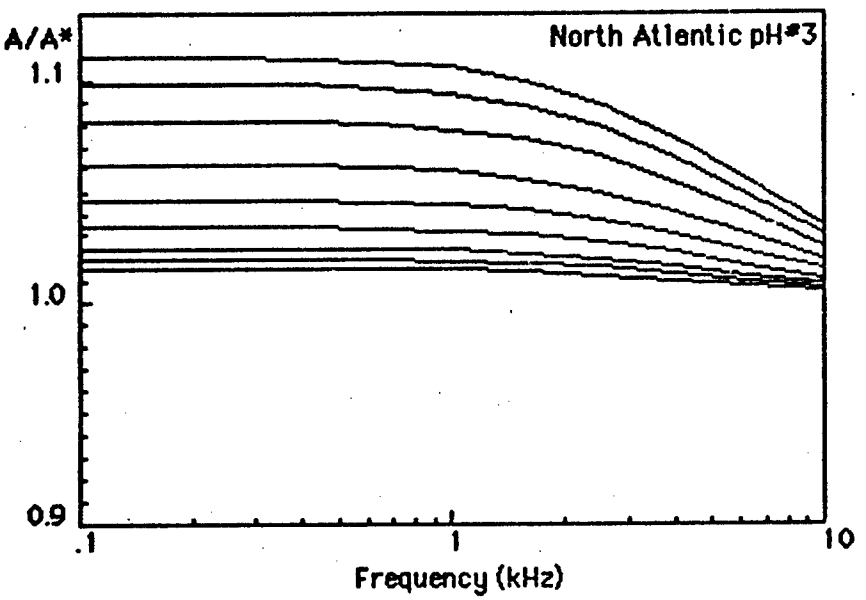

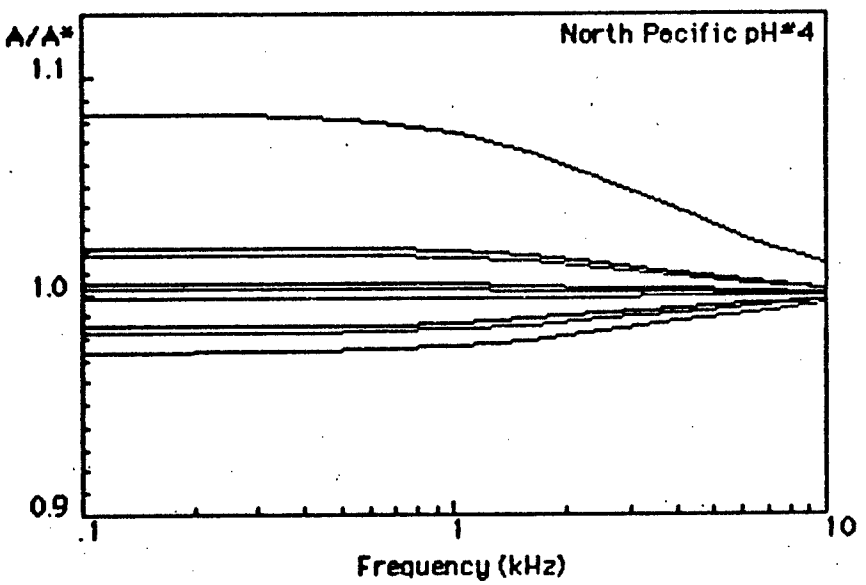

Figure 42: Absorption ratio A/A*.

Figure 42 shows the effective values of A/A* where A*is calculated for the 2 km depth values of temperature and pH. In this case, errors diminish as ray angles increase while the opposite occurs if axial values are used.

At high latitudes in the Southern Ocean, profile pH*1 is the appropriate model and errors for this case are roughly doubled compared to the case of profile pH*3. Interpolation between the 2 km and axial values in the ray analysis would clearly help to keep the errors within acceptable limits.

Global Model

$$A = A_1(MgSO_4) + A_2(B(OH)_3) + A_3(MgCO_3)$$

$$A_n = (S/35)\, a_n f^2 f_n / (f^2 + f_n^2)$$

$$a_1 = 0.5 \times 10^{-D(km)/20} \qquad f_1 = 50 \times 10^{T/60}$$

$$a_2 = 0.1\ K \qquad f_2 = 0.9 \times 10^{T/70}$$

$$a_3 = 0.03\ K \qquad f_3 = 4.5 \times 10^{T/30}$$

Figure 43: Global model absorption formula.

Variability of pH is clearly the major limiting factor in the accuracy of the absorption formula. In Figure 43, the pH parameter $K = 10^{(pH-8)}$ has been substituted in the simplified absorption formula. Salinity dependence has been taken as S/35 with the caveats noted. An interim model is proposed for estimating effective K values for specific propagation modes.

Based on the analysis of the previous section, the recommended method is to use axial values of K and temperature T (°C) for the sound-channel mode and the 2 km depth values for the CZ mode. Errors at higher latitudes can be reduced by interpolating between the two values, depending on the ray paths involved. Temperature is not a problem since it can be easily be derived from the SVP if not directly available from XBT data.

Contours of pH for the surface and for the 0.5 km and 1 km depths are shown in the World Ocean Atlas of Gorshkov [27]. Contours for 2 km depth are also included in Vol. 2. Since the contour intervals are 0.1 pH unit, interpolation is required. Correction to *in-situ* pressure is also necessary.

Pressure-corrected pH data from the GEOSECS report have also been used in the analysis, allowing estimation of the 2 km contours in regions of the Pacific Ocean not covered by the Russian work. Discrepencies between the data sets in other regions have been arbitrarily resolved by adjustment of the contours so as to minimize effects on estimation error. Considerable subjectivity is obviously involved.

The K contours on the sound-channel axis in Figure 44 are based on an analysis of the Russian pH contours by Lovett [28]. The 2 km depth and surface contours derived from the Russian report are shown in Figures 45 and 46, respectively. All have been modified in taking the GEOSECS data into account.

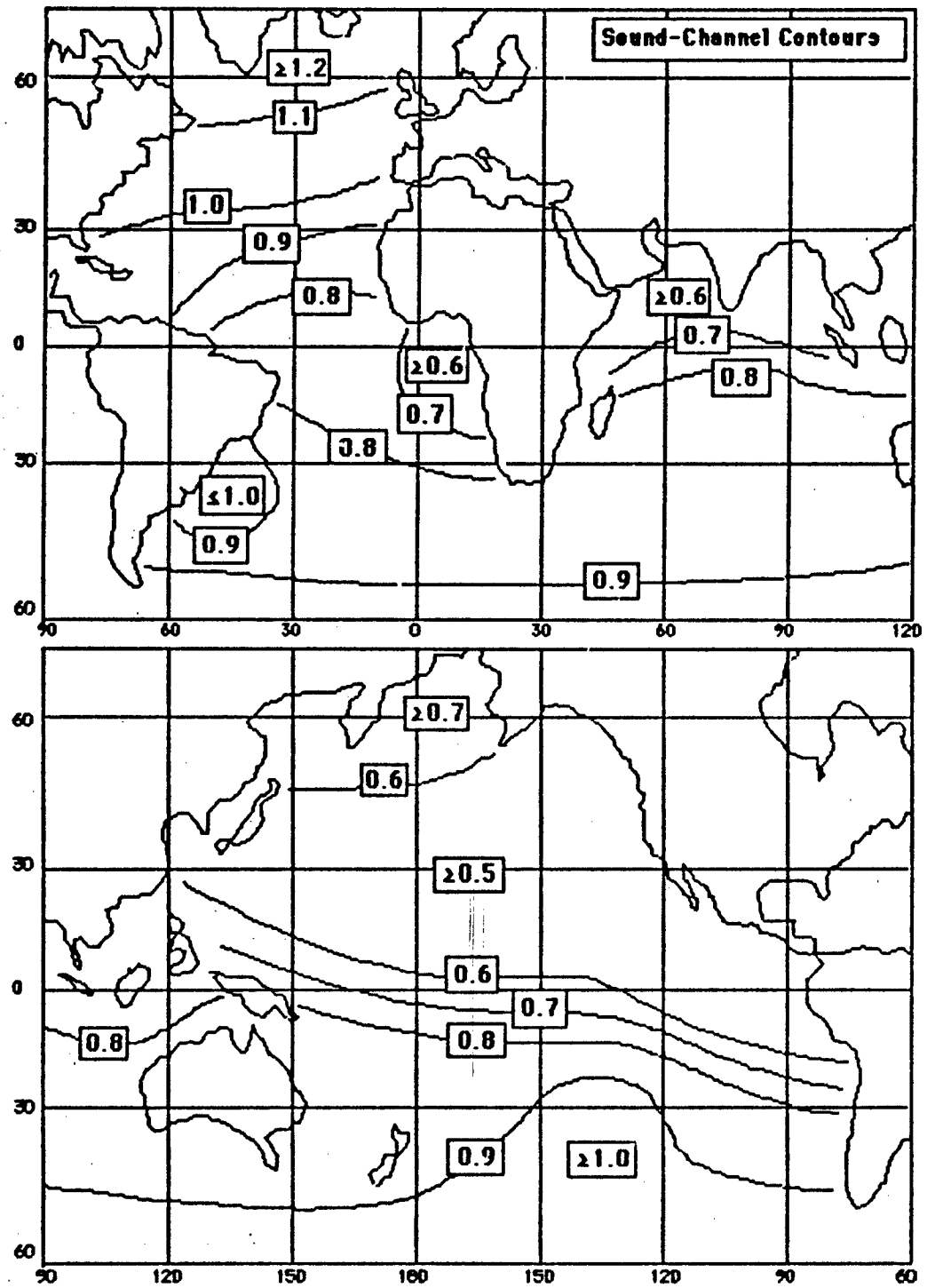

Figure 44: Sound-channel K contours.

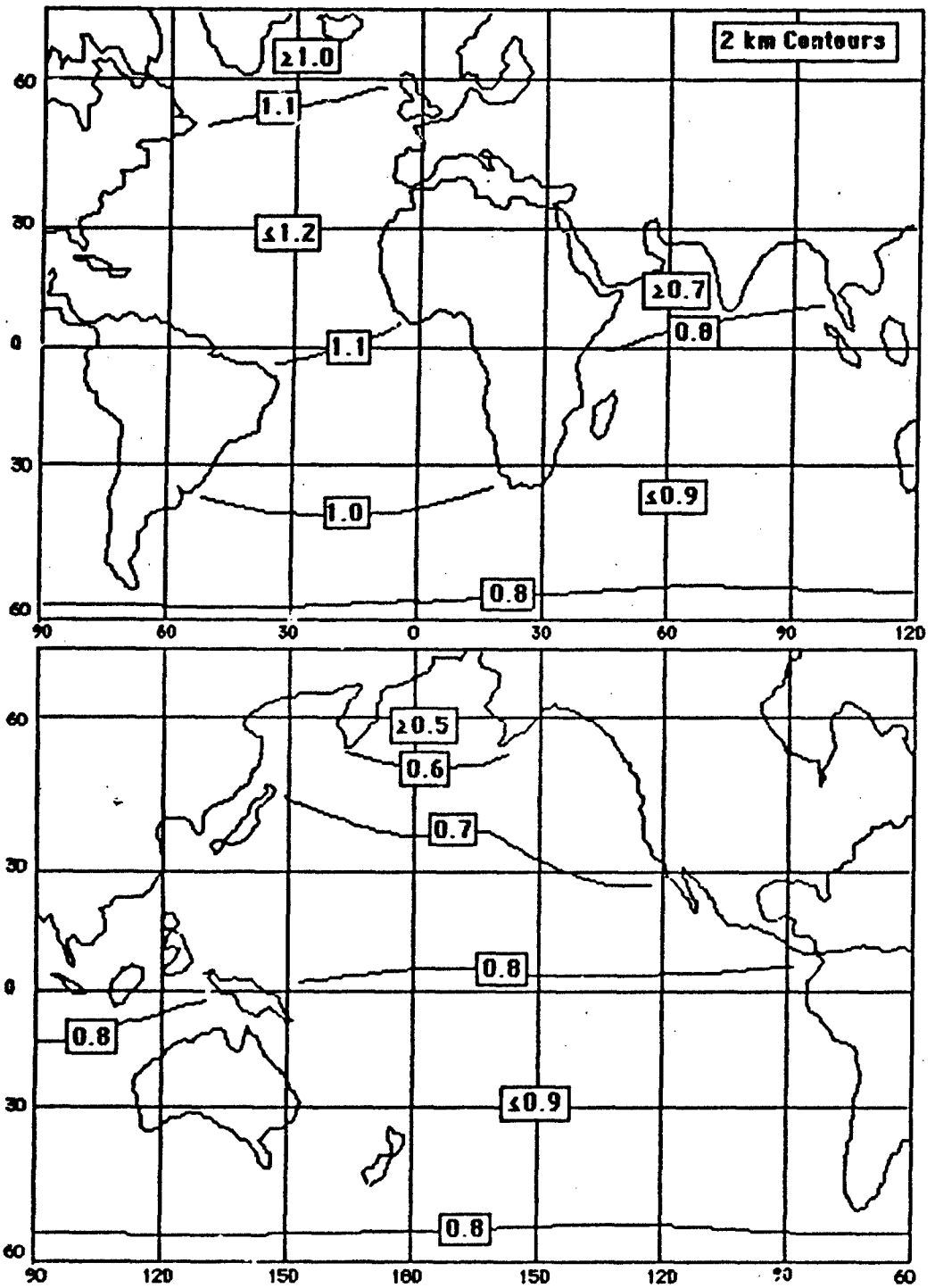

Figure 45: K contours at 2 km depth.

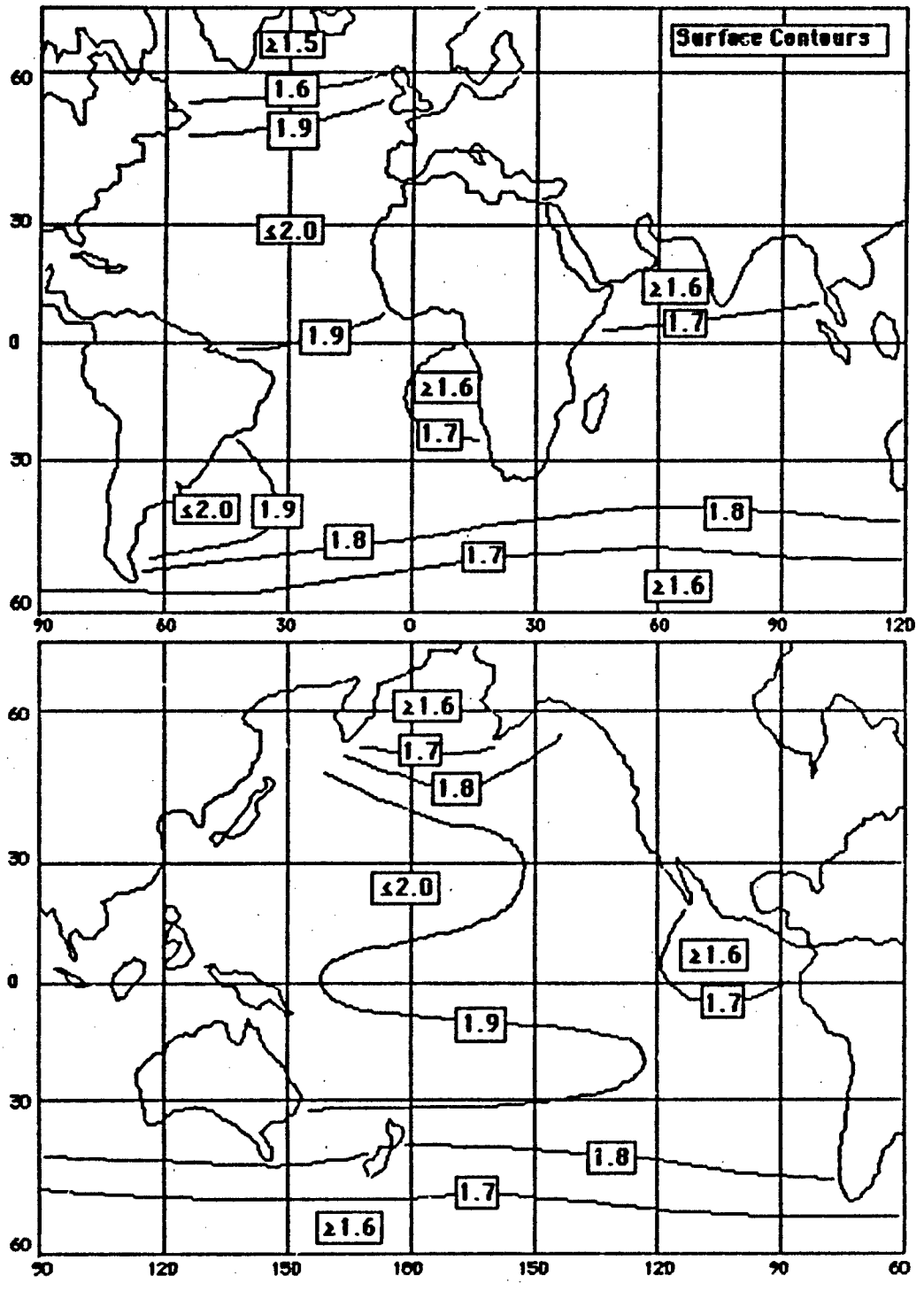

Figure 46: Surface K contours.

Conclusions and Recommendations

The three-component absorption model appears to be firmly established by NUSC laboratory and sea experiments. In addition, independent studies at the Academia Sineca laboratory confirm the results in detail [29,30].

The proposed simplified model has been shown to give very satisfactory field predictions within the error limits imposed by the environmental data. Future refinements may require slight adjustment of the parameters; however, the overall accuracy seems to be adequate for current purposes.

The main limitation of the global model is the accuracy of the pH values. Depth-dependence does not appear to be the critical factor. The simplified model uses axial values for the sound-channel mode and 2 km depth values for the other modes. Approximation errors are evidently smaller than the uncertainty in the absolute values except at the higher latitudes where interpolation between 2 km and axial values will help improve accuracy.

The K contours provided in this report should give reasonably accurate approximations for absolute pH effects in most of the World Ocean. The possible exceptions are regions where significant discrepencies between Russian and GEOSECS values have been noted.The Russian data represent local averages of archival data and tend to be lower and more variable. Errors involved in interpolating the data can also be significant.

The scope of this report has been limited to development of a suitable absorption model, a method of predicting the pH effects, and a rationale for incorporation into existing propagation models. Analysis has shown that the estimated overall accuracy ±15% of the absorption model can only be realized if the pH error is ±0.05 units or less and this remains the crucial factor. Portions of the GEOSECS pH data have been used to analyze profile effects, to supplement the missing Russian 2 km contours and to modify the others where indicated. Significant disagreements with the Russian data have been noted. It is therefore recommended that the entire GEOSECS data set be analyzed for the purpose of either refining the K contours or devising a more accurate data-base format.

At sea, the simplest solution is to measure surface pH. Measurement of the pH profile along with the normal XBT would, of course, help to resolve all the uncertainties. Since no suitable apparatus seems to be available for this purpose, development of an expendible pH probe may be indicated.

Surface scattering is another loss mechanism that can be important in surface-duct and other RSR propagation modes. Previous estimates of scattering loss vs waveheight have been based largely on surface-duct experiments. Inaccurate absorption models may cause the effects to be seriously overestimated and reassessment using the improved absorption model is also recommended.

References

1. R. H. Mellen, T. Akal, E. H. Hug and D. G. Browning, Low-frequency sound attenuation in the Mediterranean Sea", J. Acoust. Soc. Am. 78 S70 (1985)
2. E. B. Stephenson, "Transmission of sound in sea water: Absorption and reflection coefficients and temperature gradients", NRL Report S1024 (1935)
3. L. N. Liebermann, "Origin of sound absorption in water and in sea water", J. Acoust. Soc. Am. 20 868-873 (1948)
4. R. W. Leonard, P. C. Combs and L. R. Skidmore, "Attenuation of sound in synthetic sea water", J. Acoust. Soc. Am. 21 63 (1949)
5. O. B. Wilson and R. W. Leonard, "Measurements of sound absorption in aqueous salt solutions by a resonator method", J. Acoust. Soc. Am. 26 223-228 (1954)
6. G. Kurtze and K. Tamm, "Measurement of sound absorption in water and aqueous solutions of electrolytes", Acustica 3 33-48 (1953)
7. M. Eigen and K. Tamm, "Sound absorption in electrolytic solutions due to chemical relaxation", Z. Electrochem. 66 93-121 (1962)
8. M. Schulkin and H. W. Marsh, "Sound absorption in sea water", J. Acoust Soc. Am. 34 864-865 (1962)
9. W. H. Thorp, "Deep ocean sound attenuation in the sub and low kilocycle-per-second region", J. Acoust. Soc. Am. 38, 648-654 (1965)
10. W. H. Thorp, "Analytic description of the low-frequency attenuation coefficient" J. Acoust. Soc. Am. 42 270-271 (1967)
11. C. C. Leroy, "Sound propagation in the Mediterranean Sea", in Underwater Acoustics, ed. V. M. Albers (Plenum, 1967) Vol. 2, pp. 203-241.
12. Attenuation of Low Frequency Sound in the Sea, NUSC Scientific and Engineering Studies, Volumes I & II Published by the Naval Underwater Systems Center (1981)
13. E. Yeager, F. H. Fisher, J. Miceli and R. Bressel, "Origin of low-frequency sound absorption in sea water", J. Acoust. Soc. Am. 53, 1705-1707 (1973)
14. R. H. Mellen and D. G. Browning, "Variability of low-frequency sound absorption: pH dependence", J. Acoust. Soc. Am. 61, 704-706 (1977)
15. V. P. Simmons, "Investigation of the 1 kHz sound absorption anomaly in sea water", Ph.D. thesis, University of California, San Diego, CA (1975)
16. R. H. Mellen, D. G. Browning and V. P. Simmons, "Investigation of chemical sound absorption in sea water by the resonator method", J. Acoust. Soc Am. Part I, 68, 246-257 (1980); Part II, 69, 1660-1662 (1981); Part III, 70, 143-148 (1981); Part IV, 74, 987-993 (1983)

17. R. H. Mellen, V. P. Simmons and D. G. Browning, "Sound absorption in sea water: a third chemical relaxation", J. Acoust. Soc. Am. 65, 923-925 (1974)
18. F. H. Fisher and V. P. Simmons, "Sound absorption in sea water", J. Acoust. Soc. Am. 62, 558-564 (1977)
19. F. H. Fisher, "Sound absorption in sea water by a third chemical relaxation", J. Acoust. Soc. Am. 61, 704-706 (1977)
20. D. V. Wylie, "Losses in surface duct propagation", Weapons Research Establishment (Australia) Technical Memorandum 1250, (1974)
21. R. H. Mellen, D. G. Browning and J. M. Ross, "Attenuation in randomly inhomogeneous sound channels", J. Acoust. Soc. Am. 56, 80-82 (1974)
22. H. G. Schneider, R. Thiele and P. C. Wille, "Measurement of sound absorption in low salinity water of the Baltic Sea", J. Acoust. Soc. Am. 77 1409-1412 (1985)
23. S. J. Candau, Laboratoire de Spectronomie et d'Imagerie Ultrasonores, Universite Louis Pasteur, 67070 Strasbourg Cedex, France.
24. R. W. Bannister, R. N. Denham, K. M. Guthrie and D. G. Browning, "Project Tasman Two: Low-frequency propagation measurements in the South Tasman Sea", J. Acoust. Soc. Am. 62 847-859 (1977)
25. A. C. Kibblewhite, N. R. Bedford and S. K. Mitchell, "Regional dependence of low-frequency attenuation in the North Pacific Ocean", J. Acoust. Soc. Am. 61 1169-1177 (1977)
26. GEOSECS Atlas, International Decade of Ocean Exploration (NSF), Superintendent of Documents, U. S. Government Printing Office, Washington DC 20402, Stock Number 038-000-00491-3
Vol. 1, Atlantic Expediton 1972-1973
Vol. 3, Pacific Expedition 1973-1974
Vol. 5, Indian Ocean Expedition 1977-1978
27. World Ocean Atlas, edited by S. G. Gorshkov (Pergamon Press, New York)
Vol. 1, Pacific Ocean, pp.234-235 (1974),
Vol. 2, Atlantic and Indian Oceans, pp234-235 (1978)
28. J. R. Lovett, "Geographic variation of low-frequency sound absorption in the Atlantic, Indian and Pacific Oceans", J. Acoust. Soc. Am. 67 338-340 (1980)
29. Qiu Xinfang, Jiang Jiliang and Wan Shimin, "Sound absorption in sea water due to low frequency chemical relaxations", Chinese J. Acoust. 2 71-80 (1983)
30. Qiu Xinfang, Jiang Jiliang and Wan Shimin, "Investigation of the mechanism of sound absorption by the boric acid relaxation in sea water", Chinese J. Acoust. 3 51-63 (1984)

EXTERNAL DISTRIBUTION LIST

Addressee	No. of Copies
CINCLANTFLT	1
CINPACFLT	1
COMMANDER SECOND FLT	1
COMMANDER THIRD FLT	1
SURF FORCE LANT	1
SURF FORCE PAC	1
SUB FORCE LANT (CDR Callahan)	1
SUB FORCE PAC (Staff Oceanographer)	1
TRAINING COMMAND LANT	1
TRAINING COMMAND PAC	1
SUBMARINE GROUP 2 (LT Arango)	1
SUBMARINE GROUP 6 (CDR Dantzler)	1
SUBMARINE DEV GROUP 1	1
SUBMARINE DEV SQUADRON 12 (CDR W. Stephenson)	2
DEFENSE TECH INFO CENTER	1
CNO – NOP-095, NOP-951, NOP-952, NOP-953, NOP-098 NOP-981, NOP-987, NOP-02, NOP-21, NOP-22, NOP-03, NOP-62	12
CNR – OCNR-00, OCNR-10, OCNR-11, OCNR-12, OCNR-122, OCNR-124, OCRN-125, OCNR-127, OCNR-13, OCNR-20	10
OFFICE OF NAVAL RESEARCH DETACHMENTS	1
ONR DET BAY ST. LOUIS	1
ONR DET BOSTON	1
ONR DET PASADENA	1
NAIR-03	1
SPAWAR-00, PDW-124, SPAWAR-05	3
SEA-62, SEA-63	2
NRL	2
NRL DET CHESAPEAKE	2
NRL UND SOUND REF DET ORLANDO	2
NRL SPEC PROJ DET PT. MUGU	2
NORDA	2
NEPRF	2
NADC	2
NCSC (Ms. A. Bagnell)	2
NOSC	2
NOSC DET HAWAII	2
NPRDC	2
DTNSRDC	2
DTNSRDC CARDEROCK LAB	1
DTNSRDC ANNAPOLIS LAB	1
DTNSRDC ACOUS RES DET BAYVIEW	1
DTNSRDC DET BREMERTON	1
NUSC	1
NUSC NEWPORT LAB	4
NUSC NEW LONDON LAB	2
NUSC DET AUTEC	2
NUSC DET WEST PALM BEACH	2
NUSC DET TUDOR HILL	2
NUSC DET FT. LAUDERDALE	2
NUSC DET SENECA LAKE	2

EXTERNAL DISTRIBUTION LIST

Addressee	No. of Copies
NAVAL OCEANOGRAPHY COMMAND	2
NAVAL OCEANOGRAPHIC OFFICE	2
FLEET NUMERICAL OCEANOGRAPHY CTR	2
NTSA	1
NPS	1
NWC	1
SURF WARFARE OFFICERS SCHOOL COMMAND	1
SUBMARINE SCHOOL (Code 10, CDR Almon)	1
APPLIED PHYSIC LAB, JOHNS HOPKINS	1
APPLIED PHYSICS LAB, U. WASHINGTON	1
APPLIED RESEARCH LAB, PENN STATE	1
APPLIED RESEARCH LAB, U. TEXAS	1
MARINE PHYSICAL LABORATORY SCRIPPS	1
WOODS HOLE OCEANOGRAPHIC INSTITUTION	1
UNIV. OF CT, MARINE SCIENCES (Dr. F. W. Bohlen)	1
UNIV. OF NH, EARTH SCIENCES (Dr. F. Anderson)	1
UNIV. OF RI	1
PLANNING SYSTEMS INC (Dr. R. H. Mellen) Contract #N66604-87-M-B555	10